Bern University
of Applied Sciences

UNIVERSITÄT
BERN

Faculty of Medicine
Biomedical Engineering

Master of Science Thesis

Biophysical Modeling of Deep Brain Stimulation for Parkinson's Disease

by

Alba Segura Amil

of Valencia, Spain

Supervisor
Dr. Thuy Anh Khoa Nguyen

Institutions
Department of Neurosurgery, Inselspital Bern
ARTORG Centre for Biomedical Engineering Research, Universität Bern

Examiners
Dr. Juan Ansó
Dr. Thuy Anh Khoa Nguyen

Bern, July 2019

Abstract

Background: Parkinson's Disease is the most common neurodegenerative disorder after Alzheimer's disease, affecting 6.3 million people worldwide. It is characterized by motor and non-motor symptoms such as bradykinesia, muscular rigidity, rest tremor or dementia. Treatments consist of Levodopa medication and Deep Brain Stimulation (DBS) in advanced stages of the disease. DBS treatments usually target the subthalamic nucleus (STN) or the internal globus pallidus and require a long programming phase after the surgical intervention. Biophysical modelling of DBS can provide a better understanding of the therapy. Thus it can reduce programming times and increase treatment efficacy, benefiting both, patients and physicians.

Hypothesis: The activation of hyperdirect pathway in DBS treatments for Parkinson's disease is more effective than the activation of the indirect pathway. Besides, the beta activity in the STN is related to the fiber recruitment produced by DBS.

Materials and methods: Fiber tracking of the indirect and hyperdirect pathways was performed to diffusion weighted images of healthy subjects and Parkinson patients using DSI Studio. DBS volumes of tissue activated of 20 patients from Inselspital (Bern) were used to relate the fiber recruitment produced by the stimulation to clinical score. Besides, DBS volumes were analyzed in function of the direction of stimulation. A cortico-thalamic basal ganglia model was used to obtain the STN firing rate for different percentages of fiber recruitment.

Results: To achieve maximal clinical improvement, different proportions of the hyperdirect or indirect pathway were recruited. For the tracts obtained from the Parkinson patients, 44% of hyperdirect pathway fibers had to be recruited on median to obtain maximal clinical improvement versus 87% of indirect pathway fibers for a similar clinical effect. Contrary, for the tracts obtained for the healthy subjects, 80% of hyperdirect pathway had to be recruited on median to obtain maximal clinical improvement versus 25% of indirect pathway. The segmented contacts at the third level of the lead resulted in the best clinical score, which agrees with the findings from previous literature. The analysis of the beta activity in the STN suggested that the internal globus pallidus could be a more effective target in suppressing beta oscillations.

Conclusion: As hypothesized, the hyperdirect pathway was a more effective target to obtain the best clinical outcome in the Parkinson's patients. The corticothalamic-basal ganglia model used did not allow to obtain a good characterization of beta activity in function of fibre recruitment. Further studies with local field potential measurements are required to better characterize the connection parameters of the cortico-thalamic basal ganglia model when DBS is applied.

Keywords: DBS, hyperdirect pathway, indirect pathway, fiber tracking, VTA.

Acknowledgements

First, I would like to thank Dr. Thuy Anh Khoa Nguyen, who gave me the opportunity of working in the fascinating world of brain tractography. Your guidance and support have been essential in pursuing the objective of this Master Thesis. Thanks to the Neurosurgery department of Inselspital for providing me with the patients data.

I would like to thank my family for their encouragement to continue in the good and not so good moments during all my educational stage. No matter the distance, you are always there. *Papá y mamá, gracias por darme todas las oportunidades que estaban a vuestro alcance y guiarme en el camino de la mejor forma posible. Este trabajo ha sido en gran parte gracias a vosotros.*

Finally, thanks to Marina and Pascal. Marina, thank you for being my back up during all these years of study in Biomedical Engineering. Pascal, thank you for your support and patience. My stay in Switzerland would have not be the same without you.

Ich erkläre hiermit, dass ich diese Arbeit selbständig verfasst und keine anderen als die angegebenen Hilfsmittel benutzt habe. Alle Stellen, die wörtlich oder sinngemäss aus Quellen entnommen wurden, habe ich als solche kenntlich gemacht. Mir ist bekannt, dass andernfalls der Senat gemäss dem Gesetz über die Universität zum Entzug des auf Grund dieser Arbeit verliehenen Titels berechtigt ist.

Bern, July 3rd 2019

Alba Segura Amil

Contents

Abbreviations

ADC	Map of Apparent Diffusion Constant
CST	Corticospinal tract
DBS	Deep Brain Stimulation
DT	Diffusion Tensor
DWI	Diffusion Weighted Imaging
FA	Fractional Anisotropy
GPe	Globus Pallidus External segment
GPi	Globus Pallidus Internal segment
HDP	Hyperdirect Pathway
MRI	Magnetic Resonance Imaging
MD	Mean Diffusivity
ODF	Orientation Distribution Function
PD	Parkinson Disease
RA	Relative Anisotropy
RN	Red Nucleus
SDF	Spin Distribution Function
SMA	Supplementary Motor Area
SNc	Substantia Nigra pars Compacta
SNr	Substantia Nigra pars Reticulata
SNR	Signal Noise Ratio
STN	Subthalamic Nucleus
VTA	Volume of Tissue Activated

Chapter 1

Introduction

1.1 Background review

1.1.1 Parkinson's Disease

Parkinson's disease (PD) is a neurodegenerative disorder characterized by an early destruction of the dopaminergic neurons in the Substantia Nigra pars compacta (SNpc) [1]. The Substantia Nigra is part of the basal ganglia, a group of subcortical nuclei which are strongly interconnected with the cortex and the thalamus. The basal ganglia has an important role in motor control and is also involved in cognitive and associative functions [2, 3]. This group of subcortical nuclei will be explained in further detail in section 1.1.2.

Changes in the basal ganglia can evoke motor and non-motor symptoms. These changes can precede the motor symptoms by more than a decade [1]. When approximately 80% of the dopaminergic neurons have degenerated, motor symptoms gradually appear [4]. The motor symptoms include movement disorders as bradikinesia, muscular rigidity, rest tremor and postural and gait impairment (see Fig. 1.1).

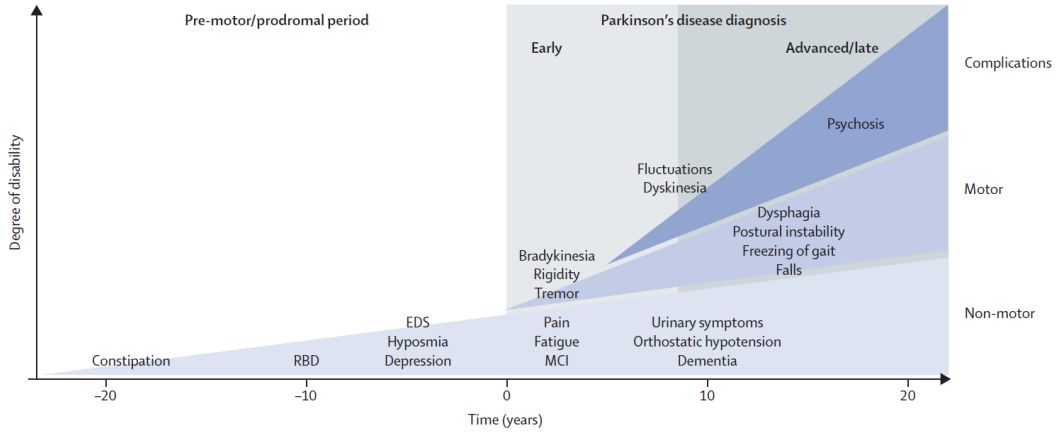

Figure 1.1. Clinical symptoms and time course of Parkinson's disease progression [1].

Parkinson disease patients can be classified according to empirical observations into two major subtypes: tremor-dominant and non-tremor dominant Parkinson's disease. Tremor-dominant PD is characterized by the relative absence of other motor symptoms while non-tremor dominant patients have phenotypes described as akinetic-rigid syndrome and postural instability gait disorder. Additionally, other patients can be classified into a third sub-group with a mix of different motor symptoms [1].

PD is the most common neurodegenerative disorder after Alzheimer's disease and it is thought to be caused by both genetic and environmental factors (see Fig.1.2)[1]. Nowadays there are no diagnostic tests at the early stages of the disease and its progression is characterized by worsening of motor features due to Levodopa resistance as well as treatment-related complications, psychosis and dementia. In the late stages, PD leads to severe disability and finally mortality.

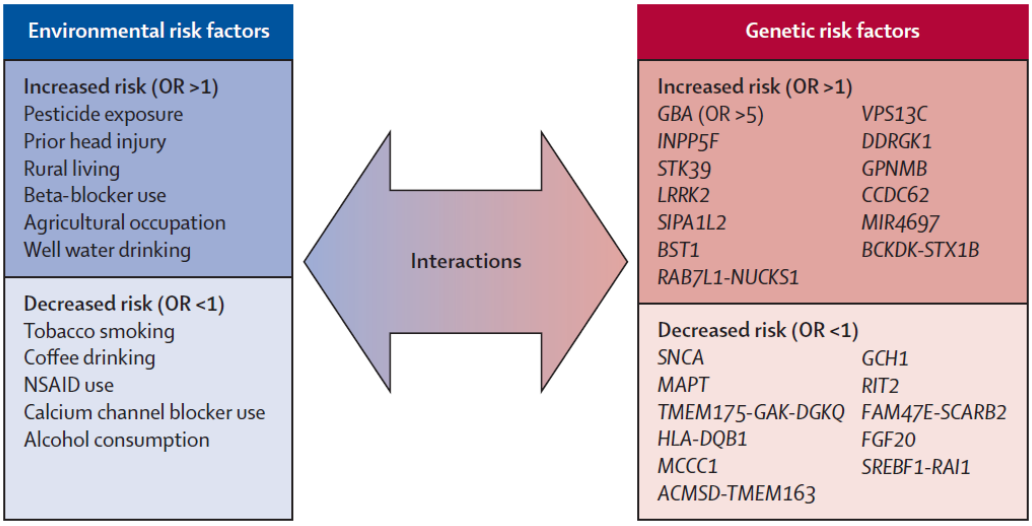

Figure 1.2. Environmental and Genetic risk factors for the development of Parkinson's disease [1]. From epidemiological and genome studies, environmental exposures and genetic risks factors that increase (OR >1) or decrease (OR <1) the risk of developing Parkinson's disease respectively. OR=odds ratio.

It is estimated that 6.3 million people worldwide have PD, with an age onset usually over 60. But approximately 1 in 10 are diagnosed before the age of 50 and some patients can be diagnosed in their 40's and earlier. In Europe, there are approximately 1.2 million people with PD: 260,000 in Germany, 200,000 in Italy, 150,000 in Spain, 120,000 in UK, 117,000 in France [5].

The incidence of PD ranges from 10–18 per 100,000 person-years; and its prevalence seems to be higher in Europe, North America, and South America (estimated crude prevalence for all ages: 66–1500 per 100,000, 111–329 per 100,000, and 31–470 per 100,000, respectively) compared with African, Asian, and Arabic countries (estimated crude prevalence for all ages: 10–43 per 100,000, 15–119 per 100,000, and 27–43 per 100,000, respectively) [1].

Other risk factors for the disease are gender, ethnicity and age. The male-to-female ratio is approximately 3:2 [6]. With respect to the ethnicity, in the USA incidence is highest in people of Hispanic origin, followed by non-Hispanic, Whites, Asians, and Blacks [7].

But age is still the greatest risk factor for the development of the disease. The prevalence and incidence increase nearly exponentially with age and peak after 80 years of age [1]. With the aging of population and rising life expectancy, the number of people with Parkinson's disease is expected to increase to between 8.7 and 9.3 million by 2030 [8]. This will affect directly the sustainability of the health systems as more people will develop the disease and will require long-term treatments.

1.1.2 Basal Ganglia

The basal ganglia comprehends a set of nuclei relevant for motor function of the body. These nuclei are divided into distinct groups according to its functionality.

The first group, striatum, includes two principal nuclei, caudate and putamen, and comprehends the input zone of the basal ganglia since their neurons are the destinations of most of the pathways that reach this complex from other parts of the brain. The destinations of the incoming axons arriving to the striatum from the cerebral cortex are the dendrites of the medium spiny neurons. The projections of the medium spiny neurons converge in the pallidum, a second structure which includes the globus pallidus and the substantia nigra pars reticulata (SNr). This second group of nuclei are the main sources of output from the basal ganglia to other parts of the brain [9].

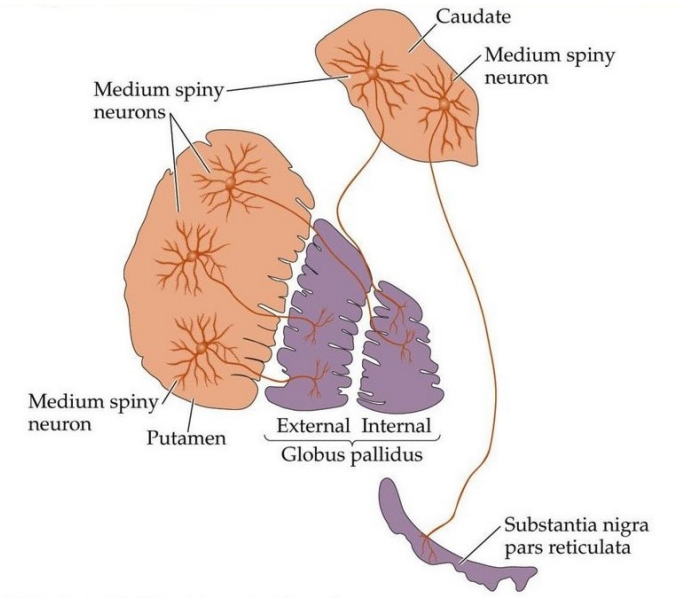

Figure 1.3. Neurons and circuits of the basal ganglia. Medium spiny neurons in the caudate and putamen [9].

The projections from the medium spiny neurons of the caudate and putamen (striatum) to the internal segment of the globus pallidus (GPi) constitute the **direct pathway** of the

basal ganglia, which facilitates the initiation of voluntary movements [9].

The basal ganglia circuits connecting the caudate and putamen (striatum) to the GPi through the external part of the globus pallidus (GPe) form the **indirect pathway**. The GPe sends projections to the subthalamic nucleus (STN) and directly to the GPi. Finally, projections from the STN will end in the GPi. This second pathway increases the level of tonic inhibition mediated by the projections neurons of the internal segment (and the substantia nigra pars reticulata), modulating the disinhibitory actions of the direct pathway [9].

The subthalamic nucleus also receives excitatory projections directly from the cerebral cortex that work together with the disinhibitory effect mediated by the projections from the external segment of the globus pallidus [9]. This cortico–STN–pallidal connection, known as **hyperdirect pathway**, has dominant excitatory effects on the output nuclei of the basal ganglia, and is faster in signal conduction from the cerebral cortex than the 'direct' and 'indirect' pathways [10].

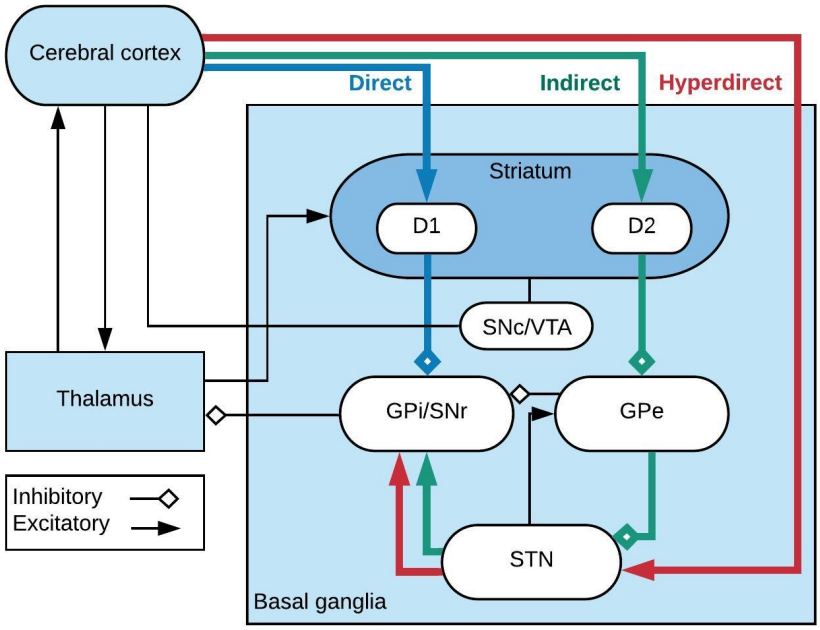

Figure 1.4. Corticothalamic basal ganglia system. Comparison of direct, indirect and hyperdirect pathways. Blue connections correspond to the direct pathway, green connections to the indirect pathway and red connections to the hyperdirect pathway.

The circuit formed by the dopaminergic cells in the substantia nigra pars compacta (SNc) has a significant influence over the integration of cortical input in the striatum. The medial spiny neurons of the striatum project directly to the SNc, which in turn sends diffuse dopaminergic projections back to the medium spiny neurons [9].

The striatum contains two inhibitory populations of medial spiny neurons, one expressing the D1 dopamine receptor and one expressing the D2 dopamine receptor [11]. This duality allows the same nigral neurons to have excitatory inputs to the spiny cells that project to the GPi (direct pathway) and inhibitory inputs to the spiny cells that project to the GPe (indirect pathway). Dopamine affects the spiny neurons by modulating their responses to the cortical input, enhancing the excitatory input from cortex through D1 receptors and suppressing this excitation with D2 receptors [9].

As mentioned in the previous section 1.1.1, Pakinson's disease is characterized by an early destruction of the dopaminergic neurons in the substantia nigra pars compacta (SNc). It is thought that dopamine depletion causes an imbalance between the two pathways, changing the excitability of D1 and D2 receptors. In the case of PD, dopamine depletion decreases direct pathway activity via D1 receptors and increases indirect pathway activity via D2 receptors. As a result, the imbalance between the two pathways will over-inhibit the thalamus [12].

High frequency deep brain stimulation (DBS) of the STN has demonstrated to reduce increased firing of the indirect pathway [13]. DBS was approved as a treatment for PD by the US Food and Drug Administration (FDA) in 2002 and since then it has been used to treat over 40,000 people with PD and essential tremor worldwide [14].

1.1.3 Deep Brain Stimulation

Deep Brain Stimulation (DBS) is a neurosurgical therapy in which a thin lead with a number of electrodes is implanted in deep brain structures of the patients, delivering electrical pulses (60-200 μs duration, 1.5 V amplitude) at a high frequency (typically > 100 Hz) to the surrounding brain tissue through one or a combination of electrode contacts [12, 11].

DBS has become an effective treatment for several movement disorders such as Parkinson's disease in advanced stages and essential tremor. Furthermore, other studies have shown its efficacy in dystonia [15], epilepsy [16] and obsessive-compulsive disorder [17].

In Parkinson's disease DBS treatments, a macroelectrode is chronically implanted in a target nucleus that can be the Globus Pallidus internus (GPi), the Subthalamic Nucleus (STN) or the ventral intermediate nucleus of the thalamus.

The leads are implanted bilaterally into the brain to achieve symmetrical results and are connected to one or two battery-powered generator units, usually near the clavicles (see Fig. 1.5). The placement of the leads requires careful stereotaxic surgery combined with radiological imaging of the patient's brain, and electrophysiological recordings of spontaneous and movement-related neuronal activity. Once the target structures are localized, stimulation is tested to determine whether the desired effects can be observed. Four to six weeks after the surgical procedure, the generator units are activated and the parameters of stimulation are fine-tuned with various combinations of pulse widths, current amplitudes and temporal patterns of pulse trains [9].

Although less frequent, adverse neurocognitive side effects may happen and negatively impact treatment outcomes. These adverse effects can be due to suboptimal placement of the electrodes or the spread of the current to surrounding structures such as the limbic system [19]. Among the possible psychiatric effects are: hypomania, which can lead to depression and apathy, and changes in behaviour and personality [20].

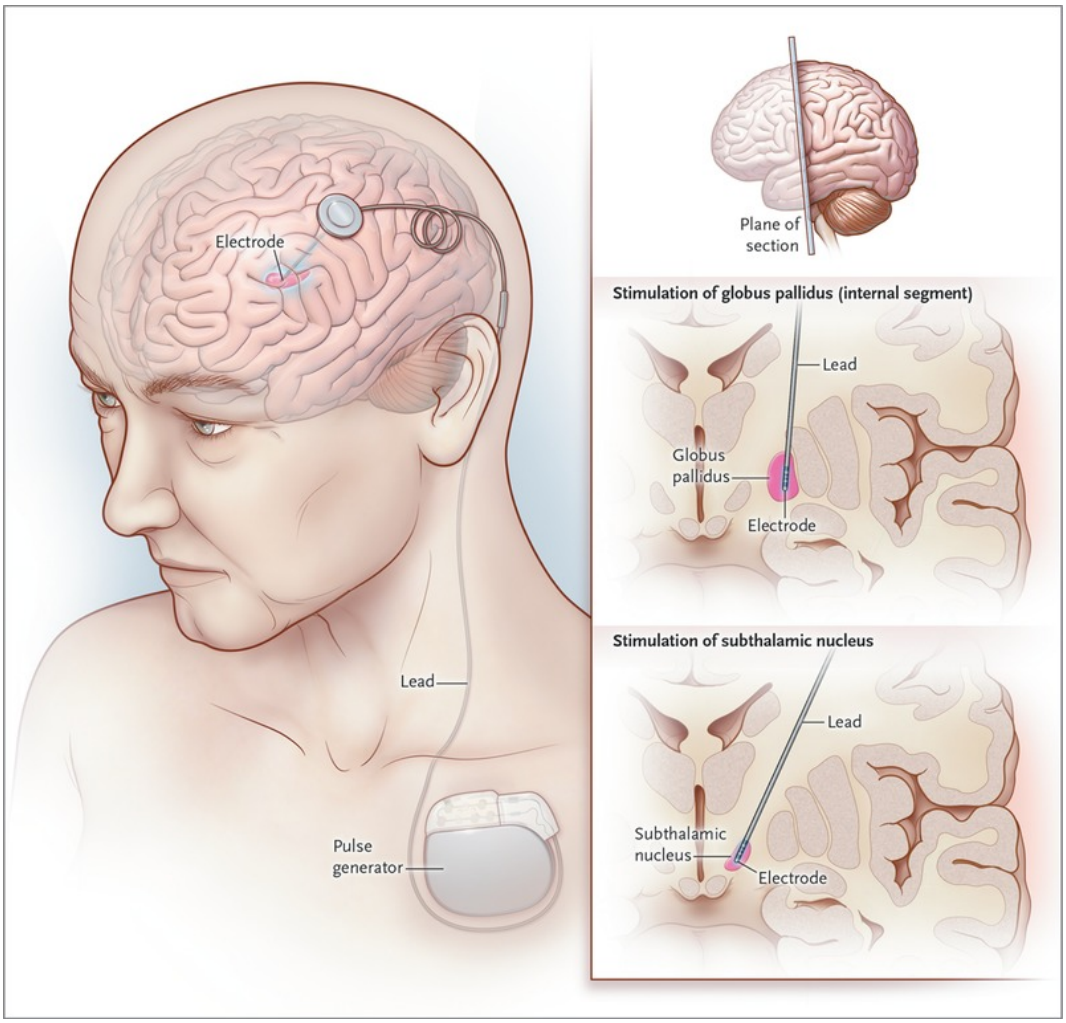

Figure 1.5. Electrode location at different sites for stimulation in DBS [18].

As mentioned above, there are different possible target nuclei that can be stimulated. Although the desired spot is the dorsolateral part of the STN (motor part), there is as well a limbic subdivison that, when stimulated, could produce psychiatric side effects. Targeting the GPi has been shown to produce less psychiatric side effects with almost equal motor improvement, although it will not be possible to reduce levodopa treatments as much as when stimulating the STN [20].

But it should be considered that the basal ganglia and cerebellum are involved in the processing of cognitive and emotional tasks and because of the stimulation spreading effects, it will be difficult to completely avoid non-motor side effects [20].

The efficacy of DBS is still to be improved with a better understanding of the underlying mechanisms of the involved specific brain circuits under physiological and pathological

conditions. In order to better comprehend these therapeutical mechanisms, combining computational modeling at various levels of description (from the cellular to the largescale brain networks) with in-vivo and clinical data appears to be a promising approach to identify the best and most effective stimulation parameters, electrode geometries and locations [12, 11].

1.1.4 Computational models of DBS

Parkinson's disease is characterized by an enhanced activity in the basal ganglia, thalamus and motor cortex at 4–8 Hz and 13–30 Hz. The enhanced beta band oscillations (13–30 Hz) in the STN of PD patients are thought to be related to symptom severity. Besides, a reduction in beta band power has been observed after treatments to alleviate PD symptoms such as dopamine treatments or DBS [11].

Several computational models have been developed with the objective of better understanding the role of the basal ganglia-thalamo-cortical loop and the modulatory effects of DBS [12]. Some of these studies suggest that the circuit formed by the STN-GPe may be responsible for the beta activity generation [21, 22] and that that these oscillations are amplified by the cortical STN inputs [23].

A first approach is to study the activity of the basal ganglia at the neuronal level. These are single neurons models describing membrane dynamics, which have been used to describe normal and pathological neuronal behaviour as synchronized oscillations. These models usually include single compartment models with a determined number of neurons belonging to the studied populations (e.g., 16 STN neurons, 16 GPe neurons, 16 GPi neurons, 2 thalamo-cortical neurons) [12].

The combination of multi-compartment neuron models with finite element models has been used to study DBS responses in small neuron assemblies and the distribution of the electrical field. These models have shown a dissociation of the activity at the soma relative to the axon during extracellular stimulation, and a systemic activation of axons both efferent and afferent to the stimulation site [11].

The multi-compartment single cell models require large amounts of computational power so, to reduce the model's dimension, a mean-field approach incorporating connectivity STN-GPe patterns from neuroanatomy can be used. In this second case, the activity of each structure is described by a distribution of membrane voltages [12]. By averaging microscopic structure and activity, it will be possible to analyze large-scale neuronal dynamics. These neural field models have already provided good results in the study of brain activity as sleep stages, eyes-open and eyes-closed in walking, nonlinear seizure dynamics, anesthesia and other phenomena. In the case of Parkinson's disease, these models have been able to account for changes in the 4–8 Hz and 13–30 Hz oscillations [11].

More advanced models as the one proposed by Müller et al. [11, 24] include DBS to potential stimulation sites such as the STN and GPi. This model aims to develop a population level description of the cortico-thalamic-basal ganglia system that can reproduce the already existing experimental observations characteristic of PD. The model includes DBS input to the STN and GPi to study how DBS stimulation suppresses or diminishes the pathological beta activity [11, 24].

1.1.5 Diffusion Tensor Imaging

Magnetic resonance imaging (MRI) allows to visualize brain structures and detect lesions in the central nervous system (CNS) non-invasively. This technique is widely used in neuroscience research and clinical diagnostics due to its versatility to provide soft tissue contrasts. There are several modalities of MRI: proton-density, T1-weighted, T2-weighted, diffusion weighted (see Fig. 1.6) [25].

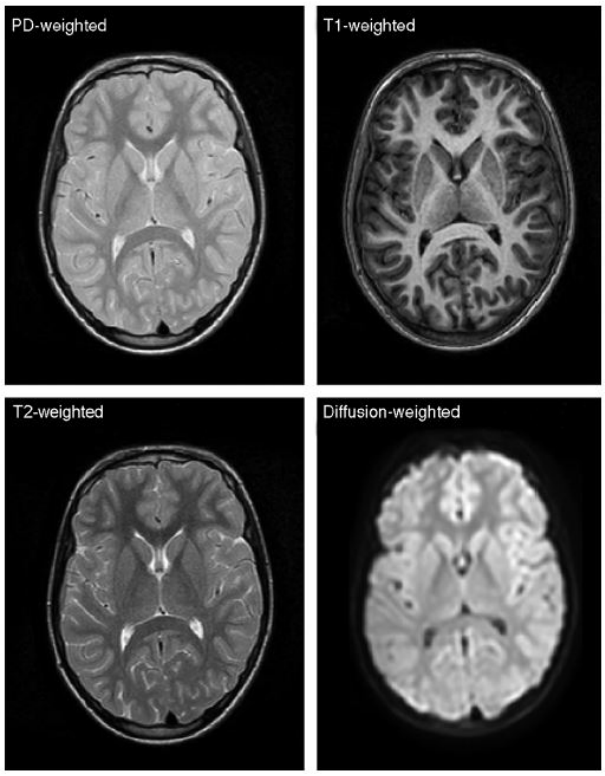

Figure 1.6. Axial proton density-weighted (PD-weighted), T1-weighted, T2-weighted, and diffusion-weighted images acquired from one healthy adult volunteer [25].

Although the contrast between grey matter and white matter in the diffusion weighted images (DWI) is not as sharp as in other modalities, this image modality can be used for the evaluation and monitoring of stroke and edema in the CNS, where the diffusion of the water molecules of the affected tissues is compromised [25].

DWI is based on the diffusion of water molecules. Water molecules inside biological tissues move randomly due to its internal kinetic energy. But biological structures such as the cell membranes and myelin sheath can restrict or hinder the movement of these molecules [25]. Furthermore, diffusion of water molecules is not equal in all directions being lower when measured perpendicular to the fiber direction rather than parallel to it [26].

At a fixed temperature, the rate of diffusion can be described by the Einstein equation:

$$< r^2 >= 6Dt$$

where $< r^2 >$ refers to the mean squared displacement of molecules, t is the diffusion time and D is the diffusion constant. The diffusion constant relates to the average displacement of a molecule over an area to the observation time. Its value depends on the particular substance being measured. Higher values of D will indicate more mobile water molecules in the medium [27].

To measure water diffusion, a pair of diffusion-sensitizing gradients are added to a T2-weighted spin-echo sequence to construct a diffusion-weighted pulse sequence. The diffusion gradients are applied along the same directional axis before and after the 180^{o} refocusing pulse with a time delay Δ (see Fig. 1.7) [27].

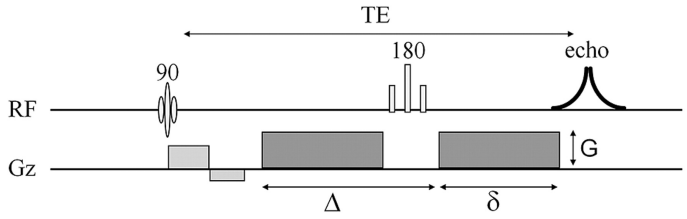

Figure 1.7. Pulse sequence diagram for a diffusion-weighted acquisition with 2 diffusion sensitizing gradients (dark gray) [27].

The diffusion effect of water molecules (spins) on MRI signals is an attenuation of the signal intensity due to incomplete rephasing of water proton spins, which change positions when applying the two diffusion-sensitizing gradients. The attenuation of the signal reflects the statistical distribution of spin displacement for each voxel [27, 25].

As a function of the strength, duration and temporal spacing of the diffusion sensitizing gradients, a b factor (s/mm^2) is determined as a measure of diffusion weighting. The signal attenuation in a voxel increases with higher b values. Typical clinical b values are between 600 and 1500 (s/mm^2).

By comparing the images acquired with diffusion gradient pulses (diffusion-weighted) and the ones acquired without diffusion gradient pulses (non-diffusion-weighted), a map of apparent diffusion constant (ADC) is calculated. This value characterizes the water molecules diffusion along a particular axis and depends on the geometrical configuration of the diffusion barriers for water molecules. To characterize the water molecules diffusion in three dimensions, ADC has to be measured along multiple axes [25].

Water molecules diffusion can be characterized as isotropic (diffusion is equal in all directions) or anisotropic (diffusion of water molecules is not equal in all directions) [27]. To quantify the direction and anisotropy of water molecules, the concept of the diffusion tensor can be used.

A diffusion tensor, in mathematical terms, is a three-by-three, symmetric, positive definite matrix. Diffusion tensors are estimated from a minimum of seven diffusion-weighted images using regression methods, with at least one non-diffusion-weighted image and six diffusion-weighted images. For each diffusion tensor, three real, positive eigenvalues $\lambda_1, \lambda_2, \lambda_3$ and the three corresponding eigenvectors $\varepsilon_1, \varepsilon_2, \varepsilon_3$ are computed. $\lambda_1, \lambda_2, \lambda_3$ are the ADCs along the axes defined by $\varepsilon_1, \varepsilon_2, \varepsilon_3$, being ε_1 the orientation with maximal diffusion coeffi-

cient and ε_3 the orientation with minimal diffusion coefficient (see Fig. 1.8) [25].

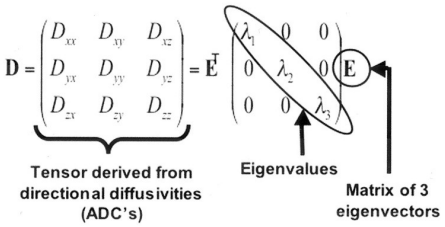

Figure 1.8. From the diffusion tensor matrix three eigenvalues $\lambda_1, \lambda_2, \lambda_3$ and three eigenvectors $\varepsilon_1, \varepsilon_2, \varepsilon_3$ are computed [28].

To visualize the diffusion tensor in three dimensions, a diffusion ellipsoid can be used (see Fig. 1.9). The shape of the ellipsoid will depend on the ratio between the three eigenvalues, determined by the tissue restriction to water diffusion (see Fig. 1.10).

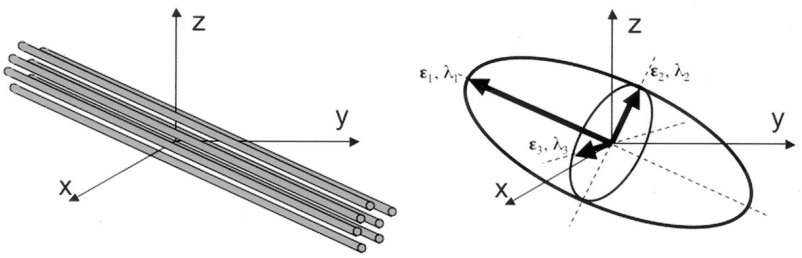

Figure 1.9. The shape of the ellipsoid will be determined by the eigenvalues while its orientation will be given by the eigenvectors of the ADC. The major eigenvalue and eigenvector $(\lambda_1, \varepsilon_1)$ will correspond to the direction of maximal diffusivity [28].

For two dimensional display, it is convenient to use scalar or vector measurements as the diffusion anisotropy. Common anisotropy indices are: mean diffusivity (MD), fractional anisotropy (FA), relative anisotropy (RA), and linear, planar and spherical anisotropy indices (CL, CP, CS) [25].

Based on the diffusion tensor concept, another MRI technique is diffusion tensor imaging (DTI), which provides information about the pathways connecting parts of the brain and the function of the cells in those pathways. Together with *tractography*, this technique is a powerful tool to study the macroscopic brain connectivity and pathology of several neurological diseases, such as sclerosis and brain damage following stroke [25].

Fractional anisotropy (FA) is the most used measure of anisotropy in DTI and it reflects the degree of directionality of the diffusion measured in a voxel. The FA value varies from 0 to 1. Low values indicate isotropic diffusion (corticospinal fluid or grey matter) while values closer to 1 indicate perfectly linear diffusion (compact myelinated white matter pathways as the corpus callosum and the corticospinal tract (CST)) [27].

When the primary eigenvalue (λ_1) is larger than λ_2, λ_3, the values of anisotropy measures as FA and RA will be high, indicating a preferred direction of diffusion [27].

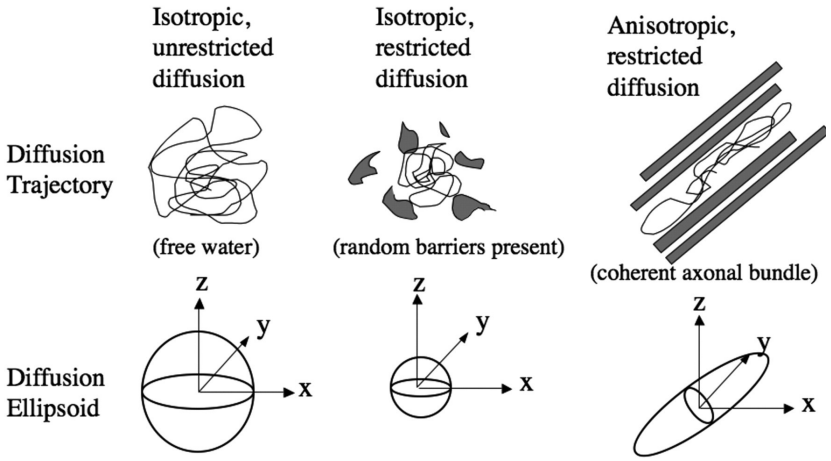

Figure 1.10. Diffusion ellipsoids for isotropic unrestricted diffusion, isotropic restricted diffusion and anisotropic restricted diffusion. Image source: [27]

The FA map can be combined with the primary eigenvector to create a coloured map showing the orientation of the primary eigenvector. Left-right oriented axonal fibers will be shown in green, anterior-posterior fibers will be shown in red and inferior-superior fibers will be shown in blue (see Fig. 1.11) [27].

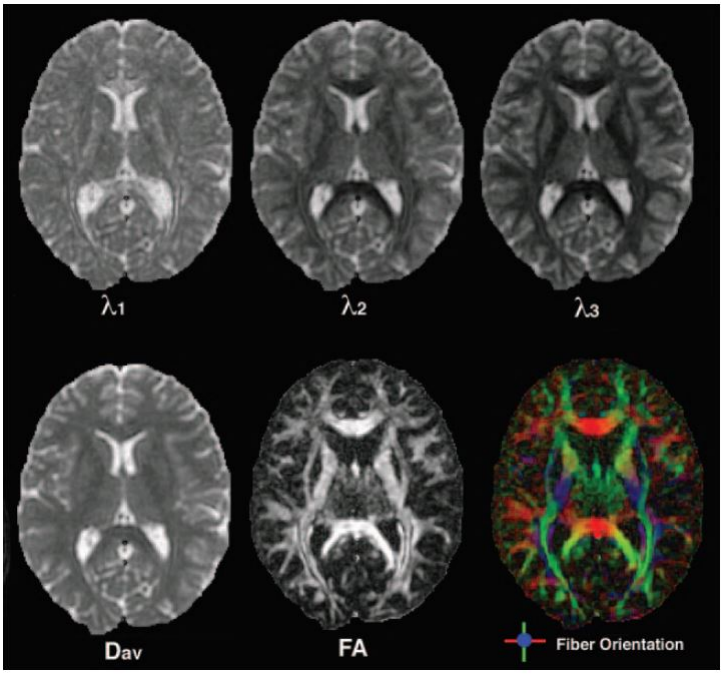

Figure 1.11. Fiber orientation map showing the orientation of the fibers. Left-right in green, anterior-posterior in red and inferior-superior in blue [27].

Diffusion tensor based models are easier to implement but have some drawbacks. The diffusion tensor only identifies a fiber orientation for each voxel, so in voxels with different orientated streamlines the tensor will not describe properly the orientation. The term *crossing fibers* is used for situations where multiple fiber orientations contribute to the signal measured for the same voxel, and anisotropy measurements such as FA are particularly sensitive to these situations [29].

Previous studies show that 60 to 90% of the voxels in white matter have crossing fibers [28]. Consequently, DT based models will be prone to errors when tracking white matter pathways containing complex fiber bundle architectures (see Fig. 1.12). In practice, the orientation produced by DT based models is reasonably close to the largest contributing fiber direction in dominant tracts such as the CST. Thus, the impact of crossing fibers will be more severe for non-dominant tracts [29].

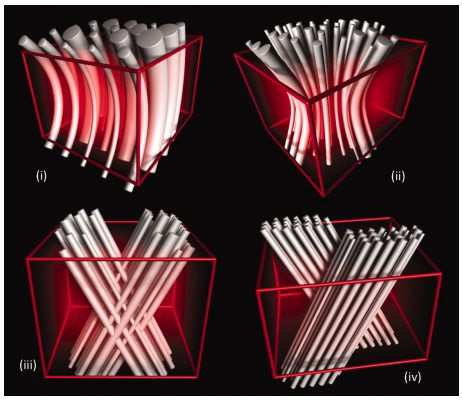

Figure 1.12. Simulated configurations of complex fiber bundle architecture at the length scale of a single voxel. Crossing fibers architectures can be described as (i) bending (e.g., uncinate fasciculus), (ii) fanning fiber bundles (e.g., pyramidal projections), (iii) interdigitating fibers (e.g., region of the centrum semiovale, where the lateral projections of the corpus callosum intersect with the corticospinal tract among others), (iv) adjacent fiber bundles (e.g., cingulum bundle and the body of the corpus callosum) [29].

More complex diffusion models with different acquisition schemes have been developed to better characterize the diffusion signal of each voxel: Diffusion Spectrum Imaging (DSI), Q-ball imaging (QBI), Spherical deconvolution and Persistent angular structure (PAS) MRI. These methods provide spherical functions as estimations of the fiber Orientation Distribution function (fODF). The fODF aims to describe the biophysical properties of the tissue and provides more insights into the underlying configuration of the fibers, quantifying the proportion of fibers along each orientation [30].

1.1.6 DTI Tractography

DTI tractography is a neuroimaging techninque which allows non-invasive study of brain structures and connectivity. The objective of DTI fiber tracking is to determine intervoxel connectivity based on the anisotropic diffusion of water molecules. This can be done by using the orientation information from the colour map and the diffusion anisotropy measurements to reconstruct axonal bundles in three dimensions [27]. DTI fiber algorithms can be divided into deterministic and probabilistic methods.

1.1.6.1 Deterministic tractography

Deterministic methods based on the diffusion tensor (DT) model initiate fiber trajectories from user-defined voxels or seeds. Fiber trajectories, also known as streamlines, follow the primary eigenvector voxel by voxel in three dimensions. When the fiber trajectory reaches the end of the voxel, the direction of the trajectory is changed to match the primary eigenvector of the next voxel [27]. Two voxels will be connected or non-connected, and each seed voxel will have only one streamline. Therefore, deterministic tractography assumes a single orientation and a single fiber in each voxel that can be determined as the maximum probability estimation of the fiber trajectory.

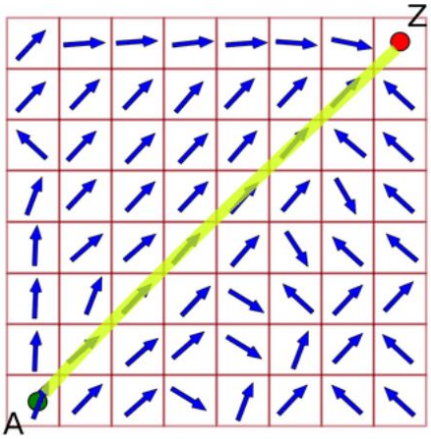

Figure 1.13. Result of deterministic tractography given by a single trajectory [31].

In these methods, it is necessary to insert constraints on the maximum turning angle of the streamline between voxels and on the minimum FA within a voxel for propagation of the streamline. Thus it is possible to constrain the streamlines to the regions where the model is actually representing the white matter pathways. Besides, the user can define regions of interest (ROIs) based on anatomical knowledge to restrict fiber tracts to areas of interest [27].

The limitations of deterministic fiber tracking are as follows [32]:

- The tracking error accumulates throughout the tracking process.
- There are problems of false continuation and premature termination.
- The connecting count between two brain regions has poor reproducibility.
- There is a crossing-branching problem.

1.1.6.2 Probabilistic tractography

Probabilistic tractography provides an estimate of the 'precision' with which a tract pathway has been reconstructed. The obtained probability values are not related to connectivity (e.g, number of axons) of the white matter pathways, but instead they reflect the confidence that the particular connection exists [29]. Therefore, probabilistic tractography algorithms iterate all possible trajectories and provide a simulated distribution of the fiber pathways [27].

The main difference with deterministic algorithms is the use of white matter orientation estimates, that are randomly drawn from the local probability density function of fiber orientations. At each step of the algorithm the direction for the next step is chosen from a range of likely orientations, instead of being unique. To obtain an estimate of the distribution of likely connections, a large number of probabilistic tracks are generated from the same seed point [29]. The probability density function of the orientation of a neuronal fiber can be estimated with an empiric function based on the FA, bayesian methods, bootstrap statistics or calibration methods [30].

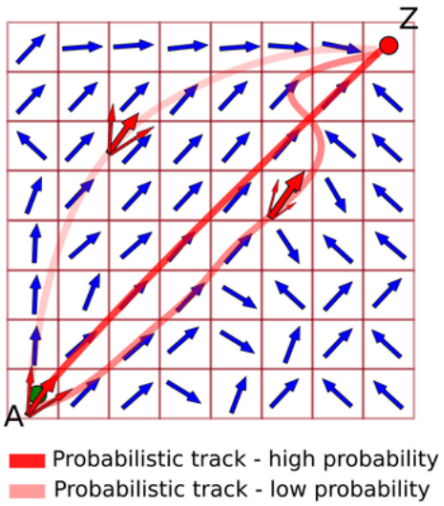

Figure 1.14. Probabilistic tracks. The result of probabilistic tractography is given by the connectivity matrix for each voxel [31].

Probabilistic tractography techniques allow the user to quantify and compare the confidence with which streamlines from a certain region might reach any different target regions. While deterministic tractography requires harsh stopping criteria, probabilistic tractography aims to go beyond uncertain regions and is more robust to noise, reducing the need for stopping criteria. Therefore, these algorithms most likely will not apply anisotropy constraints and, if any, some lenient curvature constraints [30].

Probabilistic tractography methods can define larger portions of white matter, reconstruct smaller fibers and better resolve crossing fibers, but the accuracy of these methods still depends on the information contained in the diffusion tensor and the method used to construct the probability density function [27].

Despite improved performance of probabilistic methods when delineating crossing fiber tracts compared to deterministic methods, probabilistic tractography still cannot completely overcome the limitation that the diffusion tensor model is not an adequate model for the underlying physiology in crossing fiber regions [33]. Other limitations of probabilistic tractography are that it may produce a high number of false connections and that the link to biophysics is weak [32].

1.2 Motivation

Actual DBS treatments require a long term programming which is inconvenient for patients and physicians. Two to four weeks after the placement of the leads, the stimulation programming is started. It is a time consuming manual process which requires the configuration and adjustment of several parameters during a long period of time. Besides, 20-30% of patients with implanted electrodes do not respond to the treatment.

Computational models of DBS are a promising tool to reduce programming times and increase treatment specificity. Before surgery, individualized patient models can help in the decision of whether the patient is a good candidate for DBS treatment or not, and help in the pre-surgical planning and definition of the target site. After surgery, these models could determine the best stimulating parameters according to the electrode localization and predict the patient response to the stimulation.

Diffusion tensor imaging allows a non invasive study of white matter structures and enable the study of brain development and progression of a disease. Tractography techniques based on DTI imaging provide information about the tracts that can be very useful for the planning and targeting of DBS tratments. The combination of structural information of the brain tracts with simulations of stimulation volumes can provide additional data of how the stimulation will affect the brain pathways.

Commercial programming platforms are already available but must be improved as they do not provide estimations with enough exactitude. In order to provide physicians with reliable programming tools, pathway-specific tractography and stimulation studies have to be performed to better understand and characterize the underlying connections in the brain and how they are affected by the DBS stimulation.

1.3 Objectives

The aim of the thesis is to determine if there is a fiber pathway, indirect or hyperdirect, which is more effective when activated in DBS treatments for Parkinson disease.

The first hypothesis is that the activation of the hyperdirect pathway in DBS treatments will result in a better clinical outcome. The second hypothesis is that, when applying a DBS stimulus, beta activity in the STN will decrease with the fiber recruitment of the hyperdirect and indirect pathways.

By performing a tractography study to obtain the tracts for the hyperdirect and indirect pathways, and combining the tracts obtained with simulations of activation volumes generated by DBS, it will be studied if there is a threshold for fiber activation and which stimulation volumes result in a better clinical score. Besides, a corticothalamic-basal ganglia computational model will be incorporated to evaluate how beta oscillations are related to the fiber recruitment and clinical score.

Chapter 2

Materials and Methods

2.1 Subjects images and datasets

Diffusion weighted magnetic resonance images (DWI) of healthy and Parkinson's disease subjects were used for the present study.

For the Parkinson's disease subjects, 27 image sets from the NITRC database were used. The DWIs were acquired with 120 unique gradient directions, b = 2500 s/mm^2, and isotropic 2.4 mm^3 voxels. The acquisition used a twice-refocused spin echo sequence in order to avoid distortions induced by eddy currents. All scanning parameters (b-vectors and b-values) are available when downloading the images from the website (www.nitrc.org). The database also contains demographic data of all patients such as sex, age, handedness, UPDRS scores, etc.

For the healthy subjects, a publicly available connectome was used. The connectome contains diffusion MRI data from 1021 subjects from the Human Connectome Project (2017 Q4, 1200-subject release). A multishell diffusion scheme was used for the acquisition of the images and the b-values were 1000, 2000, 3000 s/mm^2. The DWI were acquired with 90 sampling directions for each b-value. The analysis was conducted using DSI Studio (http://dsi-studio.labsolver.org) and the template file is provided when downloading the software.

Additionally, 20 patients with Parkinson's disease from Inselspital (Bern, Switzerland) were included in the study. All the 20 patients had been implanted with bilateral leads for DBS treatment. Pre-operative and post-operative scans (CT, T1-weighted MRI and T2-weighted MRI) were used to reconstruct the leads and compute the Volumes of tissue activated (VTAs). The clinical outcome corresponding to the different VTAs was available for the study.

2.2 Image reconstruction

To perform fiber tracking with DSI Studio (Jun 26 2018 build), the diffusion MRI data (NIfTI files and corresponding b-values and b-vectors) has to be reconstructed using one of the available methods: DTI, GQI or QSDR.

DTI assumes that the velocity of water diffusion follows a 3D Gaussian distribution, and the tensor calculated is the covariance matrix of the Gaussian. This type of method as-

sumes a particular diffusion distribution function/pattern and its parameters are calculated by fitting diffusion signals with the model, only requiring few samples to get the whole distribution. However, it is common that the diffusion pattern does not agree with the assumption, hence limiting the validity of the corresponding results. Besides, with complicated models, overfitting problems may happen. Nonetheless, DTI can characterize the major diffusion direction of the fibers and the reconstruction performs eigenanalysis on the calculated tensor. Anisotropy indices such as MD and FA and the three eigenvalues are exported [32].

Another approach are models which estimate the distribution of water diffusion with no assumption on the distribution. Diffusion spectrum imaging (DSI), q-ball imaging (QBI) and generalized q-sampling imaging (GQI) are examples of these model-free approaches [32].

DSI uses the Fourier transform and numerical integration to calculate the orientation distribution function (ODF) of water diffusion. The Fourier transform requires multiple b-values and multiple directions for the diffusion sampling scheme [32].

QBI uses the Funk-Randon transform or spherical harmonics to calculate the ODF, and its diffusion sampling scheme must be shell-like (HARDI acquisition, single b-value, multiple directions) [32].

GQI [34] quantifies the density of diffusion water at different orientations. This method measures the spin distribution function (SDF), a type of ODF which is the orientation distribution function of diffusion spins. GQI reconstruction offers quantitative anisotropy (QA) instead of FA. The definition for QA can be found in [34]. GQI has a great sensitivity and specificity to white matter characteristics and pathology and provides an analytical relationship between diffusion signals and the SDF. It can be applied to multiple diffusion sampling schemes and it is free from the error in numerical estimations [32].

This second type of methods (DSI, QBI, GQI) are not limited by a model since they do not assume a particular diffusion structure. They do not have the overffiting problems of the DTI approach and the calculation is less affected by outliers because it does not require complicated optimization or fitting. But these methods require more diffusion samplings to get a robust estimation (60 samplings compared to the 6 samplings and the b0 that DTI requires) [32].

A generalization of GQI, Q-Space diffeomorphic reconstruction (QSDR) allows to reconstruct SDF in the MNI template space to analyze group differences. As GQI, QSDR can be applied to DTI data, multi shell data, DSI data, none-shell-non-grill data or a combination of the previous diffusion schemes. In QSDR, DSI Studio will first calculate the quantitative anisotropy (QA) mapping in native space and then normalize to the MNI QA map. The R-squared value between the subject QA and MNI map is also calculated. This value will be an indicator about the registration results (values greater than 0.6 will correspond to good registration results whereas lower values will indicate a possible error in the registration). To perform QSDR reconstruction it is necessary to assign a template that must match the data to be reconstructed. By default, the template used is the HCP 1021 subjects, but other templates (i.e., animal templates) can be assigned.

In this study, the diffusion MRI images of the 27 PD subjects from the NITRC database were reconstructed using QSDR. The selection of the method was motivated by the objective

of creating a template from the PD subjects. As QSDR is a generalization of GQI, it allows multiple scheme acquisitions. In addition, the obtained results are in the MNI space allowing the creation of a PD subjects template.

For the 27 subjects, a HARDI scheme was used and a total of 120 diffusion sampling directions were acquired. The b-value was 2500 s/mm2, the in-plane resolution was 2.4 mm, and the slice thickness was 2.4 mm. The diffusion data were reconstructed in the MNI space using q-space diffeomorphic reconstruction to obtain the spin distribution function [34]. A diffusion sampling length ratio of 1.25 was used and the restricted diffusion was quantified using restricted diffusion imaging [35].

For the healthy subjects, the template used did not need to be reconstructed. This template was created by the reconstruction of diffusion data from the Human Connectome Project using q-space diffeomorphic reconstruction as in [36] and the available file is the final connectome containing the data of the 1021 subjects. The DWI from the HCP were acquired with a multishell diffusion scheme and the b-values were 1000, 2000, 3000 s/mm^2. The number of diffusion sampling directions were 90 for all b-values. The in-plane resolution was 1.25 mm and the slice thickness was 1.25 mm. The diffusion data was reconstructed in the MNI space using q-space diffeomorphic reconstruction [36] to obtain the spin distribution function [34]. A diffusion sampling length ratio of 2.5 was used, and the output resolution was 1 mm.

2.3 Selection of Regions of Interest (ROI)

As explained in section 1.1.1, Parkinson's disease is caused by changes in the basal ganglia. These changes produce an imbalance in the direct, indirect and hyperdirect pathways resulting in an increased connectivity to the STN.

Previous computational models have shown that the connection between the GPe and STN is essential for the appearance of beta oscillations [22], which have been related to PD symptoms and severity. The connection between GPe and STN affects the indirect and hyperdirect pathways (see Fig. 1.4) and to better understand the effects of DBS on these pathways, a tractography study was performed.

To obtain the fiber tracts corresponding to the indirect and hyperdirect tracts, different masks were used. DSI Studio incorporates several atlases containing delimited regions from previous studies. Using these regions, it was possible to create masks delimiting the regions of interest (ROI), regions of avoidance (ROA), end regions or terminative regions.

The ATAG atlas was used to establish the regions corresponding to the basal ganglia (see Fig. 2.1), and a sensorimotor cortex mask from the Automated Anatomical Labeling atlas (AAL) was used to determine the region of interest in the cortex. The SMA region from the AAL atlas included both the supplementary motor area (SMA) and the pre-supplementary motor area (pre-SMA) [37].

The indirect pathway was tracked with the fibers that originate in the sensorimotor cortex and pass through the striatum and GPe to finally end in the STN (see Fig. 2.2a), while the hyperdirect pathway was tracked with the fibers that originate in the sensorimotor cortex and end in the STN (see Fig. 2.2b). In both cases, the GPi and and red nucleus (RN) were established as regions of avoidance (Table 2.1).

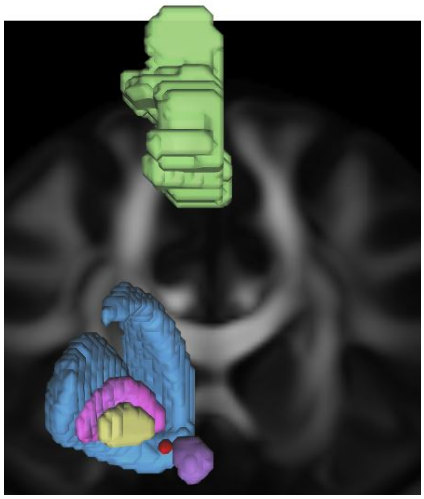

Figure 2.1. Basal ganglia structures from the ATAG atlas. The striatum is shown in blue, the GPe in pink, the GPi in yellow, the STN in red and the red nucleus in purple. The SMA region from the AAL atlas is shown in green.

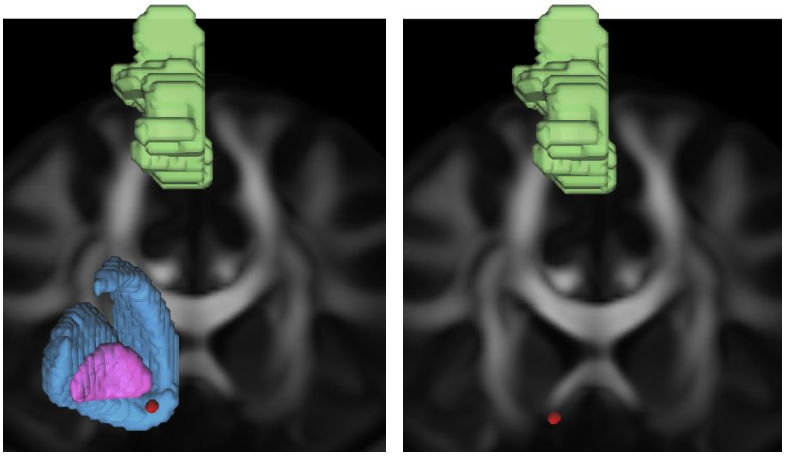

(a) Structures involved in the indirect pathway

(b) Structures involved in the HDP

Figure 2.2. Basal ganglia structures in the left hemisphere involved in the indirect and hyperdirect pathways. Structures: SMA (green), striatum (blue), GPe (pink), STN (red).

Apart from the direct and hyperdirect pathways, the corticospinal tract (CST) was obtained to visually verify that the streamlines belonging to this tract were not included in the HDP or indirect pathways. In this case, the tracts obtained start in the precentral gyrus in the cortex, go through the posterior limb of the internal capsule, through the cerebral peduncle and continue to the spinal cord (see Fig. 2.3). The atlases used were Harvard-Oxford Cortical and JHU White Matter atlas, both available in DSI Studio. The regions of interest/avoidance of the CST were placed in DSI Studio as shown in Table 2.2.

Table 2.1. Regions of interest/avoidance used to tract the indirect and hyperdirect (HDP) pathways in DSI Studio.

	Indirect	HDP	Atlas
SMA	ROI	ROI	AAL
Striatum	ROI	ROA	ATAG
GPe	ROI	ROA	ATAG
GPi	ROA	ROA	ATAG
STN	Seed	Seed	ATAG
RN	ROA	ROA	ATAG

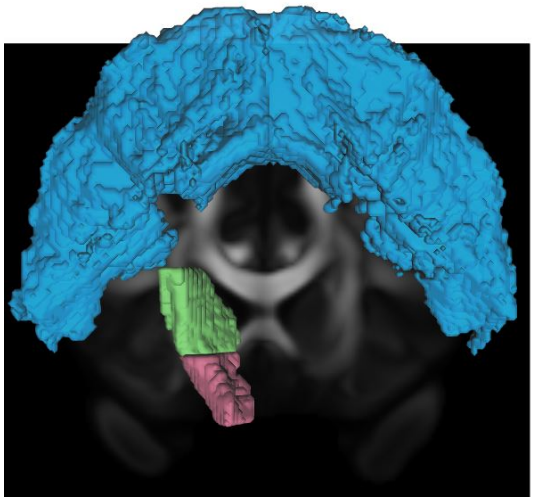

Figure 2.3. Corticospinal tract structures in the left hemisphere. Structures: precentral gyrus (blue), posterior limb internal capsule (green), cerebral peduncle (red).

Table 2.2. Regions of interest/avoidance used to tract the corticospinal tract (CST) in DSI Studio.

	CST	Atlas
Precentral gyrus	ROI	Harvard Oxford Cortical
Post. limb IC	ROI	JHU WM labels
Cerebral peduncle	ROI	JHU WM labels

2.4 Fiber tracking

Fiber tracts of the indirect pathway, HDP and CST were obtained for the group of Parkinson patients (NITRC database images) and for the group of healthy patients (HCP 1021 template) in their dominant hemisphere using the regions of interest and avoidance specified in section 2.3.

2.4.1 Tracking parameters

DSI Studio allows the user to modify the tracking parameters according to the requisites of the study. The tracking parameters used are visualized in Fig. 2.4.

The **anisotropy threshold** determines the threshold for fiber termination. In QSDR, the fiber threshold is based on the quantitaive anisotropy (QA), which is defined for each fiber orientation. The initial value is determined automatically by 0.6*(Otsu's threshold). Otsu's threshold, obtained by Otsu's method, will be the optimal separation threshold that maximizes the variance between the background and the foreground [32]. In all cases, PD images and HCP template, the anisotropy threshold used was the default value provided initially.

The **maximum turning angle** will terminate the tracking if two consecutive moving directions have crossing angle above this threshold [32]. As in similar tractography studies, [38, 39, 40], this value was fixed in 60 º.

Step size defines the moving distances in each tracking interval [32]. The value used was half of the voxel size in one dimension (half of the spatial resolution of the image). In the case of the HCP template, this value was fixed at 0.6 mm while for the PD image set the step size was 1.2 mm.

The value for the **smoothing** parameter was 0 in all cases. This parameter serves like a "momentum" and a value of 0 means that the propagation direction is independent of the previous incoming direction [32].

A *minimum* and **maximum length** was determined to filter the fibers shorter or longer than these values. For both images types, HCP template and PD image set, the minimum length was 10 mm and the maximum length 300 mm. These parameters are consistent with the expected length for the studied pathways.

Setting the parameter **Topology-Informed Pruning (TIP) iterations** to 1, 2 or 3 will allow to remove false connections using the TIP method [41]. This value was set to "3".

Seed orientation was defined as "all". This approach starts a track for each fiber orientation resolved in a voxel aiming to explore all possible connection even though it will be sensitive to noisy fibers [32].

The **seed position** was set to subvoxel. With this strategy, each seed voxel may have infinite seeding locations within the voxel.

The **interpolation method** used in estimating the fiber orientation was trilinear, and the deterministic *tracking method* was the default Euler approach.

The tracking algorithm was terminated when 5000 **seeds** were placed in the seeding area. The randomize seeding was set to "off" and no checking ending was applied.

2.4.2 Fiber tracking of Human Connectome Project template

Tractography was performed directly to the HCP 1021 template. The tracts for the three pathways (indirect, hyperdirect and CST) were obtained separately placing the regions of

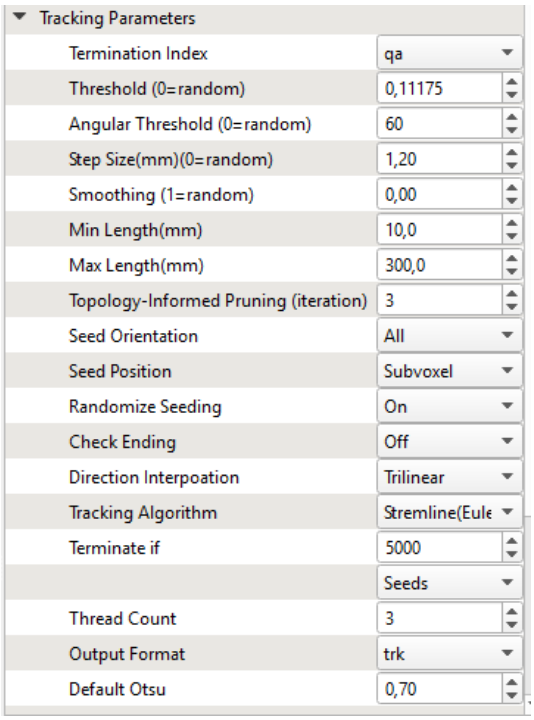

Figure 2.4. Tracking parameters used in DSI Studio to track the fiber pathways.

interest and avoidance as specified in section 2.3.

Considering that the HCP contains data from a majority of right handed patients, the three pathways were obtained only for the left hemisphere, which would be the dominant hemisphere for these subjects (see Fig. 2.5).

The tracking parameters were determined as specified in section 2.4.1. The anisotropy threshold used was 0.18618 and the step size 0.6 mm.

As a final step in the tracking, the tracts were transformed to the MNI template when exporting them from DSI Studio.

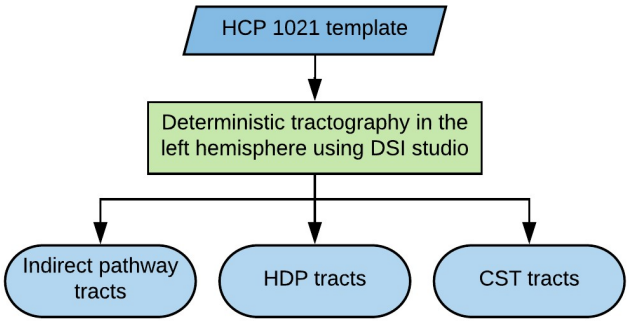

Figure 2.5. Pathway tracking in HCP 1021 template.

2.4.3 Fiber tracking of Parkinson's disease image set

The images from the PD image set were reconstructed with QSDR in DSI Studio, and the three pathways in the left hemisphere were obtained individually with the ROIs and ROAs as specified in section 2.3. Each file of the image set had a different anisotropy threshold determined automatically by DSI Studio, and the step size used for all the images was 1.2 mm.

After obtaining the tracts individually for the hyperdirect pathway, a group template was created using DSI Studio. The PD template only contains data from right handed patients that in the individual analysis had tracts for the hyperdirect pathway.

The group template was analyzed in the same way as the HCP template. As all the included patients were right handed, only tracts in the left hemisphere for the indirect and hyperdirect pathway and CST were obtained (see Fig. 2.6). These group tracts and not the individual ones were used for the post-hoc analysis. As for the HCP template, the tracts were transformed to the MNI template space for further analysis.

2.5 DBS Lead localization and VTA estimation

2.5.1 Lead localization

DBS leads were localized in the 20 patients from Inselspital using Lead-DBS software (http://www.lead-dbs.org) as in [42, 43] (see Fig. 2.7).

Postoperative CT images were linearly co-registered to preoperative MRI scans using Advanced Normalization Tools (ANTs) [44], and postoperative MRI scans were co-registered to preoperative MRI scans using SPM12 [45].

A first subcortical refinement was applied to correct possible brain shift occurred during surgery. Then, the co-registered images were normalized into standard stereotactic (MNI) space using the Advance Normalization Tools (ICBM 152 2009b Nonlinear Asymmetric) protocol available in Lead-DBS. This protocol uses nonlinear diffeomorphic normalization algorithms (SyN) where the deformation field is estimated based on a series of preoperative acquisitions and applied to all the co-registered images [46].

An additional brainshift correction was applied to obtain a more precise subcortical alignment between the subject and the template, and the results from the co-registration and normalization steps were visually verified before localizing the leads.

Electrodes were localized in the MNI space using the semi-automatic implementation PaCER [47]. If necessary, the lead's localization was refined with the TRAC/CORE (Horn 2015) module implemented in Lead-DBS Horn 2015 or manually. Finally, the contacts were identified.

2.5.2 VTA estimation

Volume of tissue activated (VTA) was estimated using a finite element method as in [43]. A volume conductor model was constructed based on a four compartment meshs with tetrahedral mesh that included grey matter, white matter, electrode contacts and insulated parts [46].

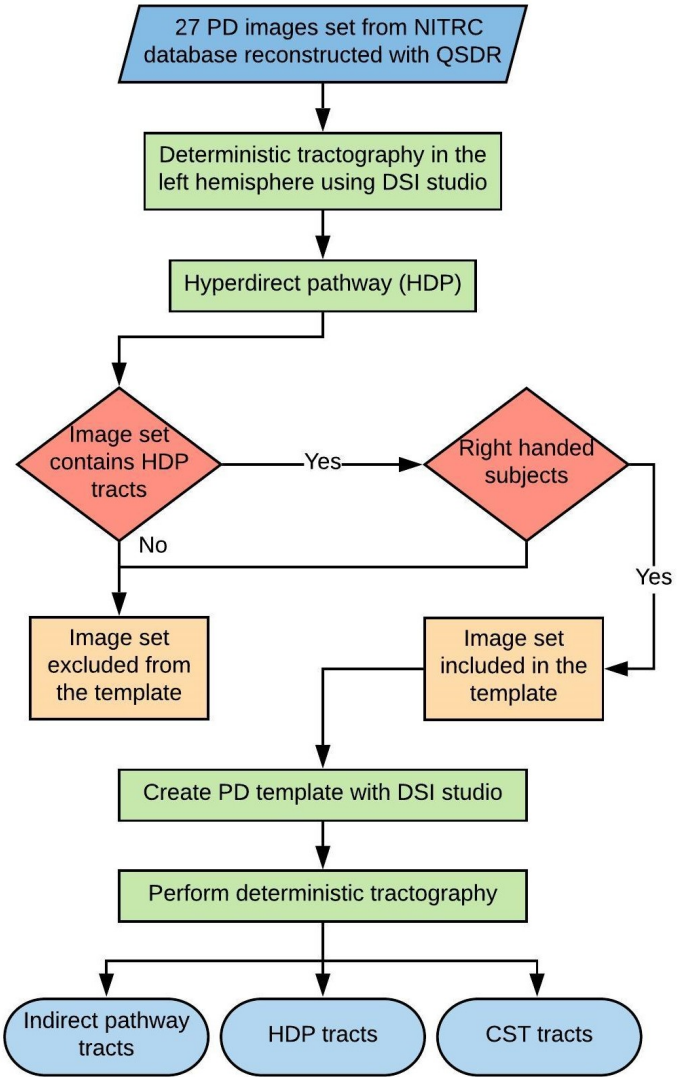

Figure 2.6. Workflow for the creation of PD template and pathway tracking.

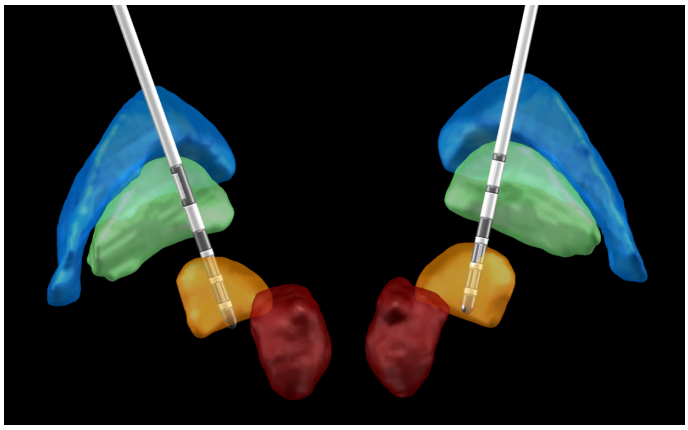

Figure 2.7. DBS leads localized in a patient MRI scan using Lead-DBS. Structures: red nucleus (red), STN (orange), GPi (green), GPe (blue).

The electric field distribution was simulated using and adaptation from the FieldTrip-SimBio pipeline [48] integrated in Lead-DBS.

The leads implanted in the patients and used for the VTA estimation in Lead-DBS were directional DBS leads (Boston Scientific, Marlborough, MA). These leads have contacts distributed along four levels with segmented contacts on levels two and three (level two: contacts 2/3/4; level three: contacts 5/6/7). Each lead contains a marker visible in CT scans which allows to identify the direction of stimulation for each contact (see Fig. 2.8).

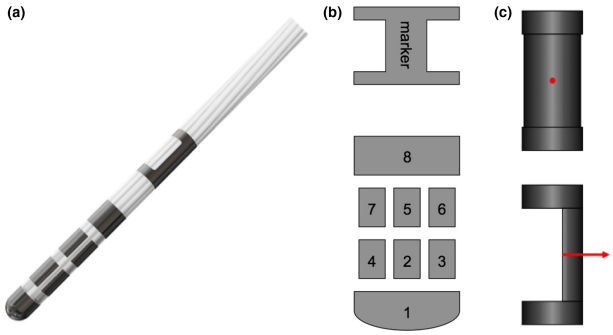

Figure 2.8. Boston Scientific directional DBS leads [49].

2.6 Fiber recruitment and clinical score

2.6.1 Fiber recruitment by VTA

The number of fibers recruited by each VTA was calculated with custom Matlab code, using the hyperdirect and indirect pathway's tracts obtained from the HCP and PD templates.

Each of the patients from Inselspital was stimulated with eight different contacts and two rings (segmented contacts on levels two and three) per hemisphere. Thus, each of the

patients had ten different VTA's calculated at effect threshold per hemisphere.

First, the tracts in MNI space calculated in DSI Studio were reorganized to match the tract format from Lead-DBS. Then, for each of the VTAs and using the Matlab function *inpolyhedron*, the tract points that were inside the volume determined by each of the VTA were calculated. The fibers corresponding to those tract points inside the VTA were identified and computed, and a percentage of the recruited fibers was obtained.

This calculation was done for the tracts of the hyperdirect and indirect pathways in both of the templates, HCP and PD. For each patient, the results provided with these calculations were the number of fibers recruited for the ten VTAs and its percentage with respect to the total number of fibers of the pathway (Table 2.3).

Table 2.3. The number of fibers recruited when stimulating with each of the VTA has been calculated using the indirect and hyperdirect pathway fiber sets.

PD / HCP template	Nº fibers recruited	% fibers recruited
$\lvert VTA_1 \rvert$		
$\lvert VTA_n \rvert$		

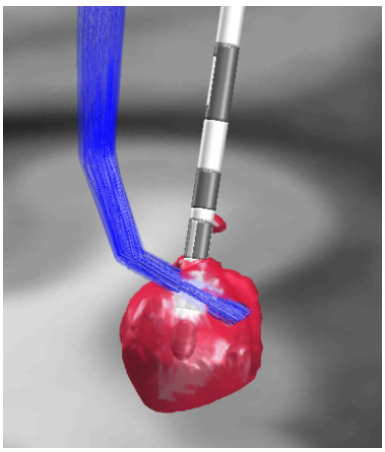

Figure 2.9. Fiber recruitment by VTA. Visualization in Lead-DBS.

2.6.2 Clinical score

The clinical score provided for the Inselspital patients contains a classification from zero to one according to the improvement experienced by the patients when stimulating with the different contacts of the electrodes. A clinical score value of zero indicates no improvement while a value of one indicates total improvement. This clinical score was based solely on testing the rigidity of the patient's hand [50].

The clinical score corresponding to each of the stimulation's VTAs has been compared to the percentage of recruited fibers to observe if there is a correlation between the recruitment and the clinical outcome (see Fig. 2.10).

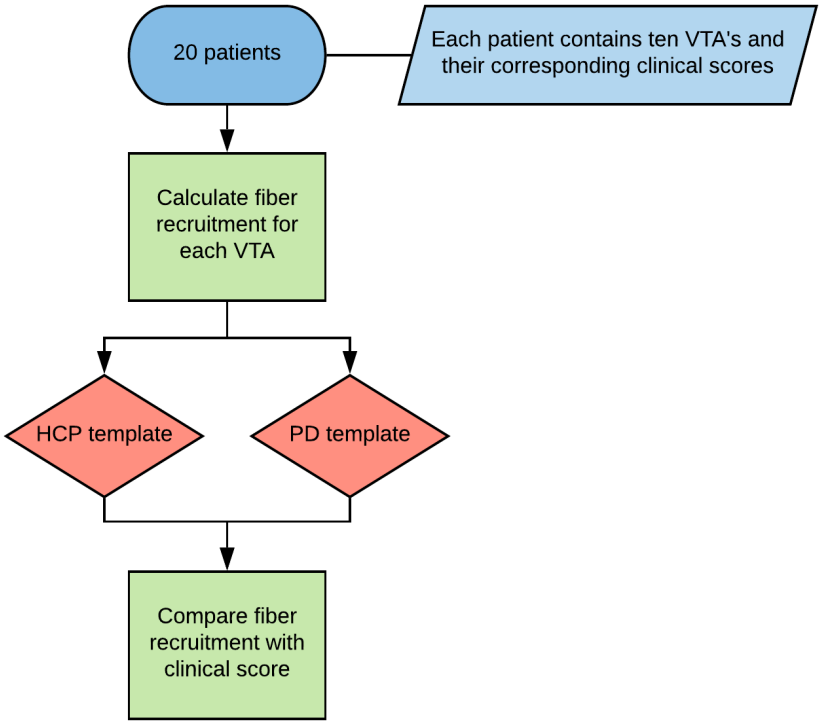

Figure 2.10. Fiber recruitment workflow.

2.7 Computational model of corticothalamic-basal ganglia system

The computational model used was developed by Müller et al. [11]. This corticothalamic-basal ganglia model includes nine neural populations of the cortex, basal ganglia and thalamus, and an input source for deep brain stimulation, x.

The cerebral cortex contains populations of excitatory pyramidal neurons, e, and inhibitory interneurons, i. The thalamus contains an inhibitory population, the reticular nucleus, r, and an excitatory population, the relay nuclei, s. The basal ganglia contains two inhibitory populations within the striatium, d_1 and d_2, expressing the D1 and D2 dopamine receptors respectively. The striatum projects to two inhibitory populations, the internal part of the globus pallidus (GPi) and the substantia nigra pars reticulata (SNr), p_1, and the external part of the globus pallidus (GPe), p_2. An excitatory population represents the subthalamic nucleus (STN), ζ. The input source x corresponding to the deep brain stimulation is connected to the GPe, GPi and STN populations (see Fig. 2.11).

The numerical simulations of the model are performed using the NFTsim code package [51]. In the model, ordinary populations (non-stimulus) have an initial firing rate and a specific sigmoidal firing response, and the axonal propagation activity is governed by the damped wave equation [11, 52].

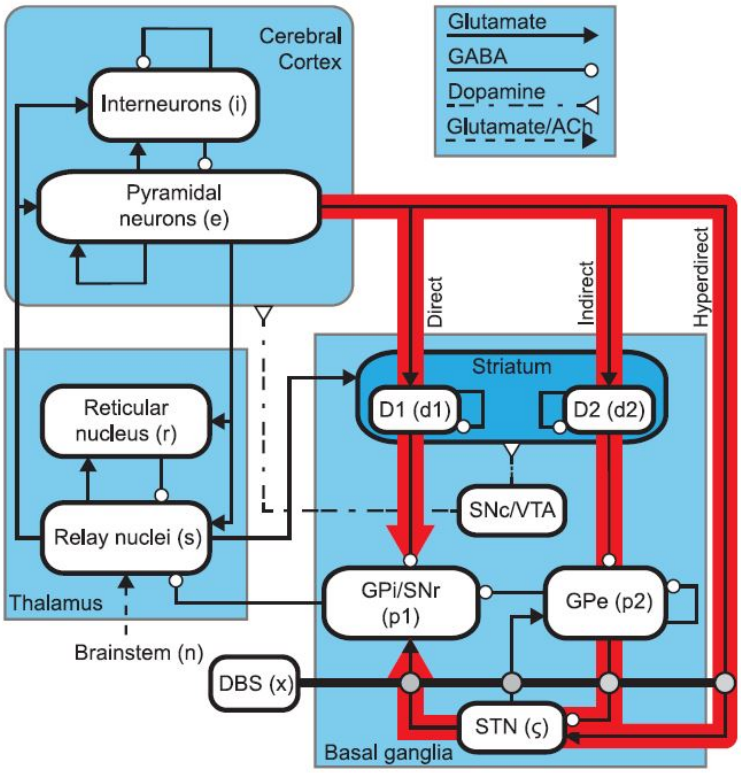

Figure 2.11. Corticothalamic basal ganglia model developed by Müller et al. [11]. The model contains populations of the cerebral cortex, (i, e), populations of the thalamus, (r, s), and basal ganglia populations in the striatum, GPi/SNr, GPe and STN, (d_1, d_2, p_1, p_2, ζ). The substantia nigra pars compacta (SNc) and ventral tegmental area (VTA) are also included in the figure indicating neural pathways affected by dopamine but are not included in the model.

For each of the connected populations, a connection strength parameter is defined as:

$$v_{ab} = N_{ab} s_{ab}$$

This parameter describes the influence of incoming spikes to population a from population b, being N_{ab} the mean number of connections between the two populations and s_{ab} the mean strength of response in neuron a to a single spike from neuron b [11].

DBS has been modeled as a stimulus population. In the same way as for the non-stimuli populations, DBS is coupled to a target population a by a connection parameter v_{ax} with a pulse frequency f_{stim}. In the model developed by Müller et al., DBS besides being coupled to STN is coupled to GPi and GPe populations as an approximation of axons terminals near the stimulation site [11].

Following the objective of this project, the firing response of the STN population has been studied. Assuming that the time scales of relevance for this study are much shorter than the time scales for significant plasticity induced change to s_{ab} in the regions of interest,

s_{ab} can be approximated as constant. Then, if N_{ab} increases or decreases so must v_{ab} proportionally. And it will be possible to infer changes in the mean connections strengths, v_{ab}.

To observe how beta oscillations vary when applying DBS, the coupling parameters v_{ax} corresponding to the connections between DBS and the target sites were modified. N_{ax} was decreased linearly from the original value in the model to zero. It was considered that the original coupling value represents the state of total fiber recruitment, while for a coupling value of zero, none of the fibers would be recruited and DBS input would not affect that population.

The DBS stimuli applied is a rectangular pulse of 20 seconds of duration with an onset at 30 seconds from the starting of the stimulation, 1 V of amplitude, 128 Hz and 2432 pulses. The mean strength parameters used for the situation of total recruitment of the fibers correspond to the ones defined by Müller et al. in [11] (see Table 2.4).

Table 2.4. Mean strength parameters for DBS input connections to the STN, GPe and GPi.

Target site	Mean strength parameter (mVs)
STN	1.086
GPe	2.4
GPi	1

Chapter 3

Results

3.1 Tractography

3.1.1 Human Connectome Project template

The tracts for the indirect and hyperdirect pathways and the CST were obtained using the HCP template as specified in sections 2.3 and 2.4.

In the case of the indirect pathway, the tracts go through the striatum and GPe before ending in the STN (see Fig. 3.1a). For the HDP, the tracts start in the primary region of the cortex reaching directly the STN (see Fig. 3.2a). The tracts obtained for both pathways correspond anatomically to the literature description.

With respect to the corticospinal tract (CST), the tracts obtained start in the precentral gyrus and traverse the posterior limb of the internal capsule and the cerebral peduncle towards the spinal cord. As expected from the literature, these tracts do not traverse the STN (see Fig. 3.3a).

3.1.2 Parkinson's disease image set

When the 27 image set from the NITRC database were analyzed individually, HDP tracts were obtained only in seven out of the 27 patients in the left hemisphere, starting in the motor area and ending in the STN. For the rest of the images, the tracts either started from anterior areas in the cerebral cortex or continued to the spinal cord, in most of the cases through the red nucleus (see Fig. 3.4).

One of the seven images containing HDP tracts in the left hemisphere corresponded to a left handed subject and consequently, this subject was excluded from the group analysis. Then, the other six image set were used to create the PD patient template.

Tracts for the indirect and hyperdirect pathways and the CST were obtained PD template in the same was as for the HCP template, as specified in sections 2.3 and 2.4.

Indirect pathway tracts obtained using the PD template are visualized in Fig. 3.1b, HDP tracts in Fig. 3.2b, and CST tracts in Fig. 3.3b. All the tracts obtained for the three pathways correspond anatomically to the literature description.

The numbers of tracts obtained for each of the pathways are visualized in Table 3.1.

(a) HCP 1021 template

(b) PD template

Figure 3.1. Indirect pathway tracts for the HCP 1021 and PD templates. Tracts start in the SMA area and pass through the striatum and GPe before ending in the STN. Structures: SMA (green), striatum (blue), GPe (pink), GPi (yellow), STN (red).

(a) HCP 1021 template

(b) PD template

Figure 3.2. Hyperdirect pathway tracts for the HCP 1021 and PD templates. Tracts start in the SMA area and end directly in the STN. Structures: SMA (green), striatum (blue), GPe (pink), GPi (yellow), STN (red).

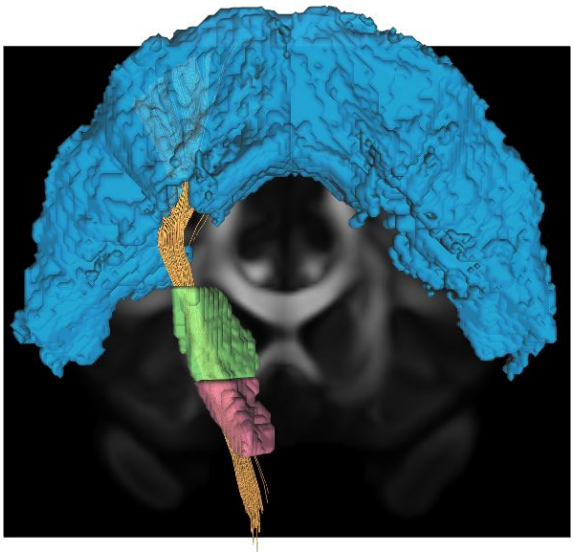

(a) HCP 1021 template

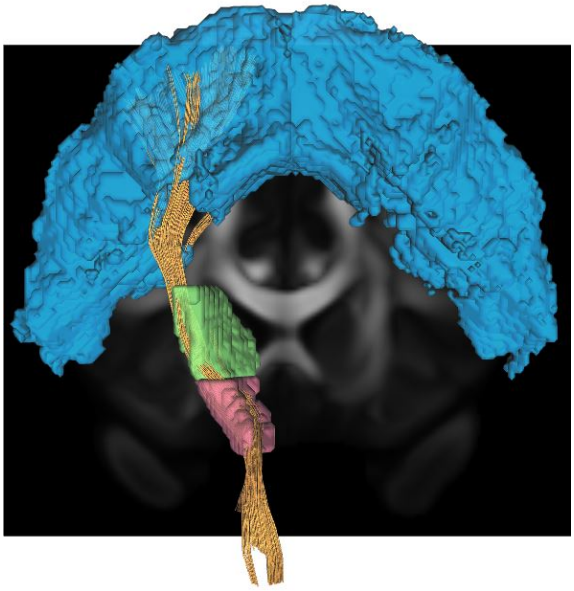

(b) PD template

Figure 3.3. The Corticospinal tract (CST) include the tracts starting in the precentral gyrus and traversing the posterior limb of the internal capsule and the cerebral peduncle towards the spinal cord. Structures: precentral gyrus (blue), posterior limb internal capsule (green), cerebral peduncle (red).

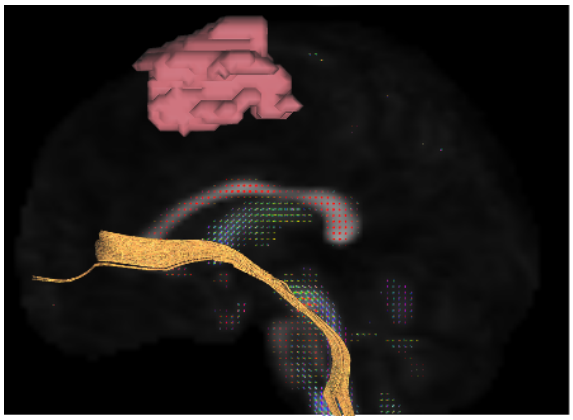

Figure 3.4. For some of the PD image sets, when tracking the HDP the results obtained were not anatomically correct. Tracts start from anterior areas in the cerebral cortex or continue to the spinal cord.

Table 3.1. Number of tracts obtained for the indirect, hyperdirect and corticospinal tracts in the HCP and PD templates.

	HCP template	PD template
Indirect	44	1079
Hyperdirect	280	326
CST	388	374

3.2 Beta activity

Data about beta activity was obtained using the corticothalamic-basal ganglia model from Müller et al. [11].

The model provides information about the firing rate of the different established populations and allows to include an external stimulus. The firing rate time series of the STN was obtained when applying an external stimulus targeting the STN at t=30 s (see Fig. 3.5 left). Besides, the power spectrum of the firing rate was calculated before and after the stimulus (see Fig. 3.5 right). As it can be observed, the power spectrum after applying the stimulus (red curve) decreases but the shape of the curve is maintained, presenting the same characteristic peaks of the beta oscillations.

Figure 3.6 shows the variation of beta activity with fiber recruitment when a DBS stimulus is coupled to different populations. For beta oscillation values, the maximum peaks in the power spectrum of the STN firing rate were considered. As explained in section 2.7, the initial coupling values in the model were modified according to the percentage of recruitment, considering the initial values as 100% of fiber recruitment.

In function of the populations that DBS stimulus was liked to, beta activity increased or decreased. Activating DBS STN-GPe increased STN firing rate while DBS STN-GPi resulted in the strongest reduction of the firing rate. Activating DBS STN and DBS STN-GPe-GPi also reduced the firing rate of the STN.

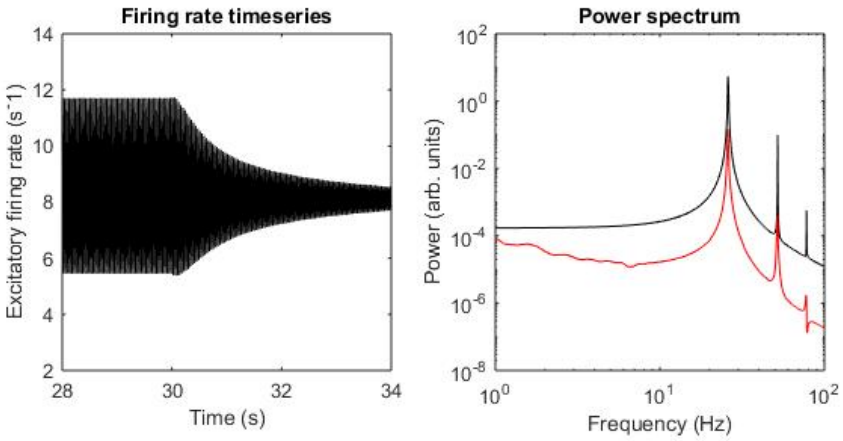

Figure 3.5. Firing rate time series and power spectrum of beta activity when applying a 128 Hz external stimulus at t=30 s using the coupling strength parameters specified in Table 2.4. In the power spectrum plot, the black curve corresponds to the power spectrum before the stimulus (t=10-30 s) and the red curve to the power spectrum after the stimulus (t=30-50 s).

Müller et al. considered that when stimulating the STN, the GPi and GPe populations were affected. When tracking fibers from a volume of tissue activated (VTA) generated for the Inselspital patients, there were fibers going through these populations. Consequently, the connections to these populations were also considered when obtaining the beta oscillations in the STN. Therefore, the beta activity data used in Fig. 3.7 corresponds to the curve where DBS stimulus is coupled to the STN, GPi and GPe.

Beta activity data for a stimulus coupled to the STN, GPi and GPe was included in Fig. 3.7 as a colour bar. It can be observed that beta oscillations are reduced when recruiting a higher percentage of fibers, as expected from the linear decreasing curve obtained in Fig. 3.6.

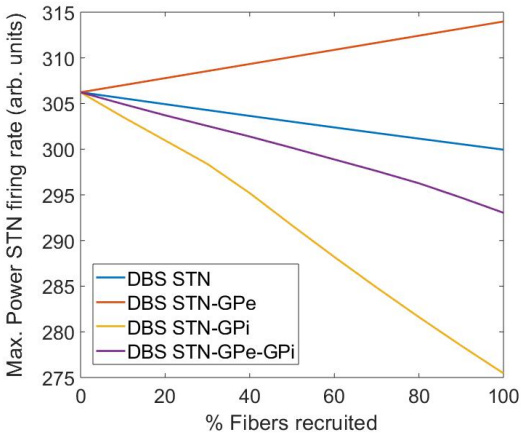

Figure 3.6. Beta activity when applying a 128 Hz stimulus at t=30 s coupled to STN, STN-GPe, STN-GPi, STN-GPe-GPi.

3.3 Fiber recruitment and clinical score

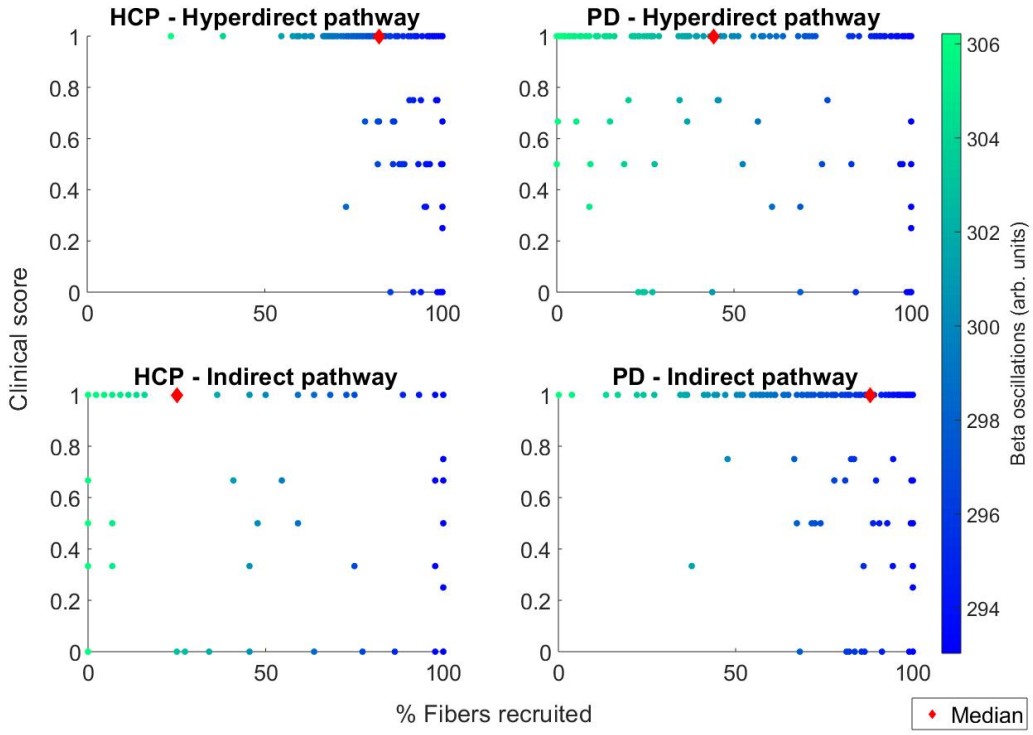

Figure 3.7. Fiber recruitment and corresponding clinical score obtained for the VTAs from the Inselspital patients. The median value of fiber recruitment has been calculated for the VTAs with a maximum clinical score. Beta activity of the STN has been included as a colour bar where dark blue indicates lower activity and green higher higher beta activity.

Figure 3.7 shows the percentage of recruited fibers for all the available VTAs (20 patients, 10 VTAs per patient at effect threshold) with their corresponding clinical score. The colour bar indicates the beta activity in function of the fiber recruitment.

The relationship between the fibers recruited and the clinical score varied depending on the connectome analyzed.

When using the tracts obtained for the healthy subjects connectome (HCP template), if the percentage of recruited fibers and their corresponding clinical score are compared, the results showed differences between the hyperdirect and indirect pathways.

For the hyperdirect pathway, there was a threshold around 50% of fiber recruitment to produce an improvement in the clinical score. Noteworthy is that fiber recruitment between 20 and 70% resulted in full improvement (clinical score equal to one), while when recruiting more than 70% of the fibers lower clinical scores appeared. However, the median value of the stimulations resulting in a maximal improvement was at 80% of fiber recruitment. This means that although exceeding the threshold of 70% resulted in lower clinical score values

for some stimulation volumes (VTAs), half of the VTAs resulting in a maximal clinical score recruited more than 80% of fibers of the hyperdirect pathway.

When considering the stimulation of the indirect pathway, a threshold of fiber recruitment could not be established. Maximum and lower clinical scores were obtained for all percentages of fiber recruitment. If only the values with the maximal clinical score were considered, the median value was at 25% of recruitment. This median value was considerably lower than the median percentage obtained for the hyperdirect pathway.

The results for the tracts belonging to the Parkinson's subjects connectome (PD template) showed some similarities and differences between the hyperdirect and indirect pathways. A threshold of fiber recruitment could not be established for the hyperdirect pathway since clinical scores equal to one were obtained for all the range of fiber recruitment. Besides, the median percentage of fiber recruitment when considering only the VTAs with a clinical score of one was at 44%. Still, lower clinical score values were distributed as well in all the range of fiber recruitment.

As for the hyperdirect pathway, maximum clinical scores were obtained for all the range of fiber recruitment in the indirect pathway. But in this case, the median value for the VTAs with a clinical score equal to one was at 87% of recruitment, considerably higher than the 44% of the hyperdirect pathway. Another difference from the hyperdirect pathway was that clinical scores lower than one started appearing at 50% of fiber recruitment. Even so, as the median value indicates, it was necessary to recruit a higher percentage of fibers to produce a significant clinical improvement.

3.4 Directional stimulation

To observe the relationship between the fiber recruitment, clinical score and direction of stimulation, each VTA was classified according to the direction of stimulation. To do so, the direction of the lead's marker was identified for each patient and the contacts generating each of the VTAs were classified according to their direction of stimulation: anterior (A), anterior-lateral (AL), anterior-medial (AM), posterior (P), medial (M), etc.

Figure 3.8 shows fiber recruitment in function of the direction of stimulation. Non-segmented contacts, contact one (C1) and eight (C8), and the two rings R1 and R2, segmented contacts 2/3/4 and 5/6/4 respectively, were considered as additional directions. Besides, the clinical score was included as a colour bar where dark blue indicates non-improvement and green indicates maximal improvement.

The results obtained for the Human Connectome Project template (HCP), in the case of the hyperdirect pathway, show that for all the directions of stimulations more than 50% of the fibers were recruited. In the case of the indirect pathway, there was a higher variety in the range of recruitment depending on the direction of stimulation.

For the tracts belonging to the Parkinson's patients connectome (PD), all directions of stimulation had a wide range of fiber recruitment in the hyperdirect pathway. In the case of the indirect pathway, except the anterior-lateral (AL) and anterior-medial (AM), the rest of directions recruited more than 20% of the fibers.

The contacts resulting in a better clinical score independently of the template used were

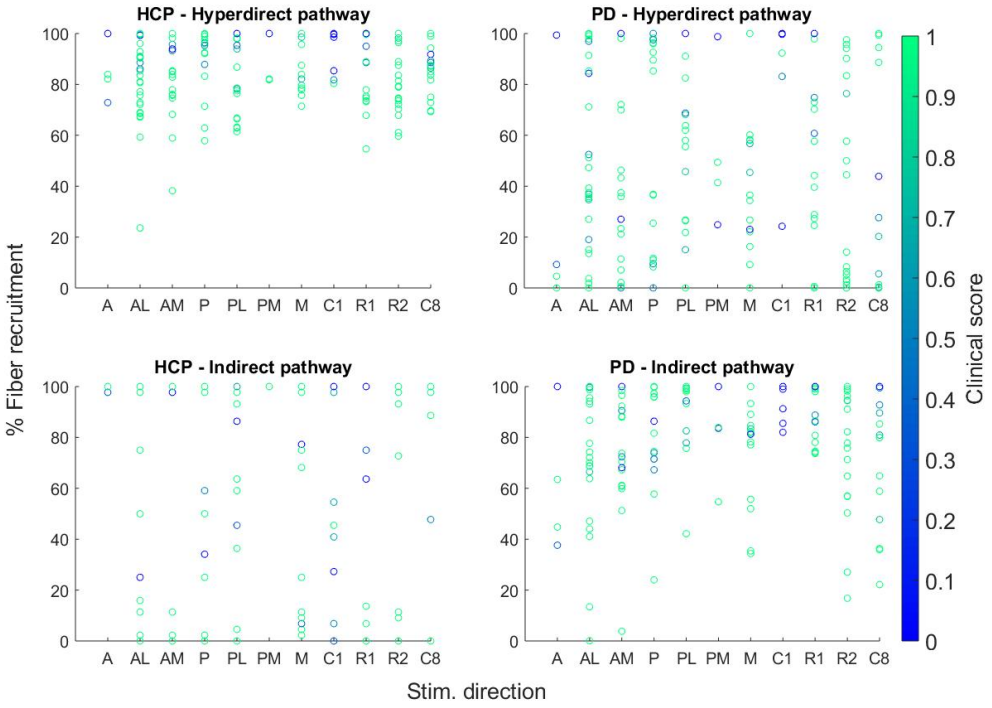

Figure 3.8. Fiber recruitment and clinical score are analyzed according to the direction of stimulation of the contact generating the VTA. Direction of stimulation: anterior (A), anterior-lateral (AL), anterior-medial (AM), posterior (P), posterior-lateral (PL), posterior-medial (PM) medial (M), contact one (C1), segmented contacts 2/3/4 (R1), segmented contacts 5/6/4 (R2), contact eight (C8).

the segmented contacts 5/6/7 which belong to the ring on the third level of the lead.

Figure 3.9 contains the box and whiskers plots of the clinical score in function of the direction of stimulation. In line with the results from Fig. 3.8, the best stimulating contacts belonged to the ring 2, with all the VTAs except one resulting in a maximal clinical score.

On the other side, the contacts stimulating in an anterior (A) or posterior-medial (PM) direction and the non-segmented contact at the first level (C1) were the ones resulting in worse clinical scores. The rest of the directions of stimulation, including the ring at the first level (segmented contacts 1/2/3) and the contact at the fourth level had a mean clinical score around 0.8.

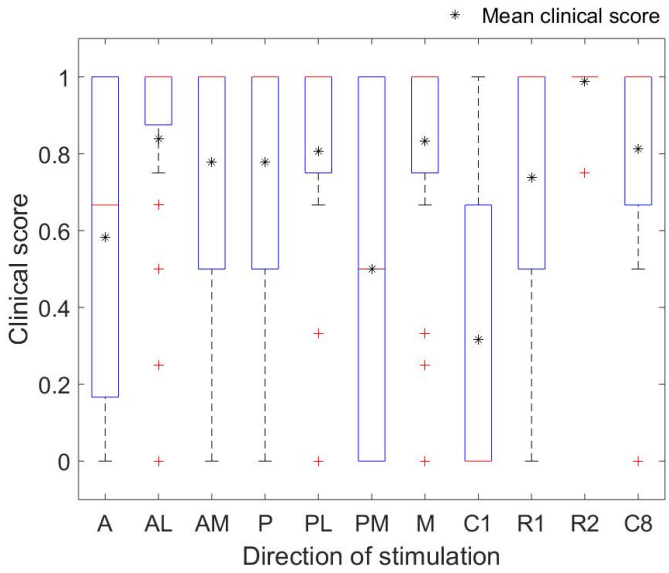

Figure 3.9. Clinical score is analyzed according to the direction of stimulation of the contact generating the VTA.Direction of stimulation: anterior (A), anterior-lateral (AL), anterior-medial (AM), posterior (P), posterior-lateral (PL), posterior-medial (PM) medial (M), contact one (C1), segmented contacts 2/3/4 (R1), segmented contacts 5/6/4 (R2), contact eight (C8).

Chapter 4

Discussion and Conclusions

4.1 Fiber tracking

The tractography results for the indirect and hyperdirect pathways and for the corticospinal tract show that it is possible to obtain independent streamlines for each of the tracts.

The study performed by Neumann et al. [53] considered streamlines passing *through* the subthalamic nucleus as tracts belonging to the hyperdirect pathway. In turn, Gunalan et al. obtained cortifugal streamlines and considered hyperdirect axons to the collateral fibers starting in nodes of Ranvier of the cortifugal streamlines and terminating in the STN [54].

In this study, only streamlines starting in the supplementary motor area of the cortex (SMA) and ending in the STN were considered as hyperdirect tracts. This approach was the same as in Petersen et al. [19], as it was considered that anatomically, the hyperdirect streamlines end in the STN.

Obtaining proper pathway tracts with DSI Studio was highly constrained or limited by the signal quality and resolution of the images. Previous versions of DSI Studio were not able to render small structures such as the STN when the scans had a resolution lower than 1.5 mm. But newer versions of DSI Studio (Jun 26 2018 build) are able to render some points belonging to the structure. However, this was still not useful and was a problem when using scans from clinical practice which had resolutions worse than 1.5 mm. In addition to not being able to render the structure, the region was not well characterized as a region of interest and the obtained tracts did not belong to the pathway of interest.

In general, DSI Studio was able to tract major pathways such as the corticospinal tract appropriately. But tracking minor pathways such as the hyperdirect pathway did not provide similarly good results.

The algorithm used to perform the reconstruction of the images influenced the tracking results as well. The tracts obtained for the hyperdirect pathway could differ significantly when using GQI or QSDR reconstruction. For some of the patients from the NITRC database, it was possible to obtain hyperdirect tracts with GQI reconstruction but not with QSDR reconstruction. On the other side, QSDR reconstruction was more robust when rendering small structures such as the STN and this allowed a better specification of the region of interest and provided better tracking results.

The different tracking results in function of the reconstruction method suggest that the diffusion information obtained with each of the methods is not exactly the same, even though QSDR is meant to be a generalization of GQI. These differences could be due to the data normalization. When reconstructing DTI scans with GQI, the data was kept in the subject's space; when using QSDR, the data was normalized into DSI Studio standard space.

The diffusion data contained in each of the individual images had a strong repercussion on the average template. If a certain pathway was obtained individually in the scans, when averaging the scans across patients, it was possible to obtain that pathway in the template. Otherwise, the averaged template would include data from scans where the pathway was not obtained and the resulting streamlines did not correspond to the anatomical definition of the pathway.

Other studies [19, 54] use probabilistic tractography instead of deterministic. Probabilistic methods are more robust to noise, are better when resolving crossing fibers and can reconstruct smaller tracts, but they produce a high number of false connections. These methods are very useful when tracking unknown pathways as they consider all possible directions for propagating streamlines. However, deterministic tractography can be accurate enough when studying known tracts.

In an international tractography competition (ISMRM 2015 Tractography challenge, http://tractometer.org), 96 tractography pipelines submitted by 20 different research groups were evaluated by comparing the tractography results to known connectivity. The study concluded that the results do not improve with higher-quality data and even when using high resolution data a considerable amount of false-positive bundles were obtained [55]. In this competition, the methods that offered the higher validation connections were GQI and DTI tractography. But it must be considered that the data used for the competition had a poor signal-to-noise ratio.

Considering images from clinical routine, it can be assumed that the data quality is not as good as in scans for research studies. For these situations, would probabilistic tracking algorithms overcome the problems derived from the noise and the low resolution maintaining an adequate ratio for valid connections? According to the results from the international tractography competition, the major limiting factor is not data quality, but the tracking algorithm used. Thus, there is still room for improvement regarding the algorithm's white matter characterization.

In the present study, the algorithm used to reconstruct the scans was QSDR, a generalization of GQI. When obtaining the tracts for the hyperdirect and indirect pathways, *manual* tract selection had to be used in order to delete some tracts which traversed the STN and continued to the spine following the corticospinal tract. But manual tract selection was just a superficial solution to the problem since the algorithm was obtaining some non-valid tracts not ending in the region of interest.

4.2 DBS of hyperdirect vs indirect pathway

As shown in Table 3.1, the number of fibers obtained for the group of healthy subjects (HCP template) was 44 streamlines for the indirect pathway, 280 for the hyperdirect pathway and 388 for the corticospinal tract. For the group of Parkinson's disease patients (PD template),

the number of tracts obtained for the indirect pathway was 1079, 326 for the hyperdirect and 374 for the corticospinal tract.

The hyperdirect pathway has strong excitatory effects on the output nuclei of the basal ganglia and its conduction is faster than for the indirect and direct pathways [10]. Thus, a higher number of tracts belonging to the hyperdirect pathway than to the indirect pathway could be expected. This occurs for the HCP template, where the number of hyperdirect tracts is six times the number of indirect tracts. But for the PD template, the streamlines belonging to the indirect pathway are three times the number of streamlines belonging to the hyperdirect pathway.

In Parkinson's disease there is an increase of the excitability of D2 expressing neurons, affecting the indirect pathway. An increase of the excitability of D2 neurons will over-inhibit the GPe, reducing the inhibitory output from the GPe to the STN and from the GPe to the GPi. As a result, the excitatory connection between the STN and the GPi is increased. The increase of the excitatory connection between the STN and GPi and the over-inhibition from the GPe to the GPi results in an increment of the inhibitory response from the GPi to the thalamus, affecting the selection of motor programs.

The imbalances in the pathways affect the neural populations in terms of increasing or decreasing firing rates, but the tractography results of the indirect pathway in PD showed an increase of the number of tracts. These structural changes would mean that new connections are being created. Following brain damage, structural changes in brain pathways generating new connections to other regions of the brain have been observed [56], but the tractography results obtained for the indirect pathway in PD indicate an increase in the number of connections for the same pathway. Further patient-specific studies with larger images dataset and using other tractography algorithms must be performed to clarify whether the increment in the number of streamlines is characteristic of the disease or if it is related to the data quality and tractography technique.

Figure 3.7 compared fiber recruitment with clinical score and beta activity. For the hyperdirect pathway, when using the HCP template, there was a threshold of 50% of recruitment to observe an improvement in the clinical score and the median percentage to obtain a maximal clinical score was at 80% of recruitment. In the case of the PD template, the improvement in the clinical score was observed for all percentages of recruitment and the median recruitment when obtaining a maximum clinical score was at 44%.

For both cases, HCP template and PD template, the percentage of fiber recruitment in the hyperdirect pathway resulting in a maximum clinical score was over the threshold of 15% of activation proposed by Gunalan et al. in [54]. In their study, they concluded that after reaching this threshold of activation, internal capsule fibers of passage started being recruited and side effects appeared. In the present study, the activation of the internal fibers of passage was not taken into account. While Gunalan et al. obtained cortifugal streamlines and divided them into two pathways, internal capsule fiber of passage and hyperdirect pathway, for this study independent hyperdirect pathway tracts starting in the cortex were obtained.

The clinical score for the Inselspital patients graded their clinical improvement after DBS stimulation. The VTAs used for the stimulation were at effect threshold, typically without persistent side effects. Thus, a relationship between activation of the hyperdirect pathway and appearance of side effects was not established.

Gunalan et al. used one patient-specific DBS pathway activation model (PAM) to calculate the biophysical response of the pathway to electrical stimulation. This type of model is more difficult to develop and analyze than the one used for the present study, where the stimulation volumes are defined around the electrode contact. The differences in the methods, to obtain the tracts and to define the volumes of tissue activated, can be a reason for the different percentages of pathway activation.

Considering that the hyperdirect pathway has a stronger influence on the basal ganglia output, targeting these tracts would have a better treatment response. Electrical [57, 58] and optogenetic [59, 60] stimulation of the hyperdirect pathway have been directly associated to therapeutic benefit in rodent models of PD.

For the PD template, for both the hyperdirect and indirect pathways a maximum clinical score was achieved when recruiting a reduced percentage of fibers. But if only the VTA's resulting in a maximal clinical score are considered, 44% of the hyperdirect pathway fibers were recruited on median versus 87% of indirect pathway fibers. These results support the hypothesis of the importance of the hyperdirect pathway since a smaller percentage of recruitment is necessary to obtain the maximal clinical score. Nevertheless, it must be considered that the number of tracts for the indirect pathway using the PD template was much larger than for the hyperdirect pathway and the stimulation volumes were the same in any case.

4.3 Beta activity in the STN

The beta activity of the STN was studied as a function of fiber recruitment with the computational model. The strength parameters connecting two populations result from the multiplication of two terms, the mean number of connections N_{ab} and the mean strength response to a single spike s_{ab}. The original strength parameters of the model were modified linearly in function of the percentage of fiber recruitment. The values proposed by Muller et al. are based on physiological estimations and, as the mean strength response s_{ab} term was not available independently from the mean number of connections N_{ab} it was considered as a constant term. Because of this assumption, the beta oscillations are minimal with a 100% of recruitment and increase with the reduction of fiber recruitment. Even though tractography studies as the one performed provide enough information to estimate the number of connections, some physiological measurements are still needed to better estimate the strength response when applying an external stimulus.

In a later study, Müller et al. evaluated the effects of DBS over the STN, GPi and STN-GPi. Their results showed that DBS-GPi is more effective than DBS-STN for suppressing beta activity in the STN, but less effective at reducing cortico-STN beta-band coherence [24]. Clinical studies of DBS-STN and DBS-GPi show simmilar motor improvements for both groups of patients, although PD medication is more reduced in DBS-STN and less adverse events occur in DBS-GPi [61]. Nonetheless, further studies are needed to determine whether the power of STN activity or the cortico-STN coherence are more correlated with PD motor symptoms.

4.4 Direction of stimulation

When the fiber recruitment and clinical score were analyzed in function of the direction of stimulation, the directions of stimulation resulting in a better clinical score were the ones

produced by the segmented contacts 5/6/7 and the anterior-lateral direction.

Herzog et al. established the dorsolateral part of the STN (motor subdivision) as the most effective site for stimulation in PD [62]. Besides, it has been observed a higher degree of beta activity near the dorsolateral border of the STN [63]. After implanting the leads targeting the STN, the location of the segmented contacts 5/6/7 at the third level of the lead corresponds to the dorsolateral part of the STN. Depending on the pathway used, the fiber recruitment generated by the VTAs varied. But the clinical score was always equal to one except for one patient, for whom it was 0.75. Therefore, these contacts were determined as the ones producing the best clinical score.

4.5 Conclusions

The tractography results provided different tracts for each of the pathways studied. Individual tracts for each pathway were obtained because different regions of interest were established for each of them. However, the resolution of DSI Studio when rendering the STN may be insufficient to clearly differentiate the tracts belonging the the hyperdirect and indirect pathways.

When incorporating the data from the VTAs, differences in the fiber recruitment of each pathway were observed. Still, with this results it cannot be established if there is one pathway that when stimulated results in a better clinical outcome.

When only analyzing the tracts obtained for the PD template, the hyperdirect pathway had a lower threshold of activation than the indirect pathway to produce a maximum clinical score. According to these results, this pathway would be a better target for DBS treatments as it requires a lower percentage of fiber recruitment to produce the maximal beneficial effects. Nonetheless, the tracts obtained for the HCP template show opposite results. In this case a higher percentage of fiber recruitment of the hyperdirect pathway has to be achieved in order to obtain the maximal clinical score, while with lower percentages of fiber recruitment of the indirect pathway the maximal clinical score was obtained.

Beta activity was analyzed in function of the fiber recruitment using the corticothalamic-basal ganglia model developed by Müller et al., and beta oscillations were minimal when all the fibers of the pathway were recruited. When modulating the coupling parameters to observe the changes in the beta activity, the three connections affected (DBS-STN, DBS-GPe, DBS-GPi) were modified linearly and likewise varied the beta activity for all the pathways. Activating DBS STN-GPi resulted in a stronger reduction of STN firing rate than only activating the STN, which suggests that stimulating the GPi is more effective for reducing the beta activity in the STN. To improve the accuracy of the model, a better estimation of the coupling strength parameters between the affected populations and the stimuli is needed.

Lastly, the direction of stimulation was compared to the fiber recruitment and clinical score. The contacts stimulating in an anterior-lateral direction were the ones resulting in a better clinical score. But even better were the results obtained for the stimulation with the three segmented contacts at the third level of the lead (R2). Considering that beta activity is directly related to PD symptoms, it is coherent that the electrodes closer to the focus of beta activity in the dorsolateral part of the STN are the ones resulting in a better clinical outcome.

Chapter 5

Outlook

The results of the tractography study showed the necessity of improving the methods for the acquisition of images, reconstruction and tracking algorithms. DSI Studio was not able to render small structures from the atlases when the images had a resolution worse than 1.5 mm and this was an important limitation when tracking the hyperdirect and indirect pathways. Although it is possible to create manual regions of interest, for non-expert users or when analyzing a large data set, the atlases are a very useful tool which allow the reproducibility of the region of interest. Thus, for further studies using clinical patient images, it must be considered that the image resolution will determine if the structure can be rendered and used as region of interest. To avoid this problem, images should have a resolution better than 1.5 mm.

It would be also interesting to reproduce the process done in the present study using probabilistic tractography. Other studies propose these methods as a better option for obtaining the hyperdirect pathway, but it would be worthwhile to observe if using the same images set, probabilistic methods overcome the problems derived from the diffusion tensor approach and maintain an acceptable rate of invalid connections.

Tracking algorithms must be improved. To improve their specificity, anatomical information from ex-vivo histological studies could be incorporated. DSI Studio eliminates automatically some of the obtained tracts, but incorporating extra anatomical information could help in the reduction of non-valid connections, specially in probabilistic methods.

Besides, considering VTAs not only at effect threshold would allow to study if there are other pathways such as the corticospinal tract that when activated are related to side effects.

With respect to the computational models, the one proposed by Müller et al. accurately reproduces the neural populations of the cortex, thalamus and basal ganglia and incorporates a DBS stimulus. However, the estimation of the connection strength parameters could be improved incorporating local field potential recordings from Parkinson patients. These measurements of the strength response to a single spike together with the number of connections obtained with tractography, would allow a better characterization of the beta activity in the STN when applying a DBS stimulus. More accurate estimates of the mean strength response to a single spike in the computational model combined with patient-specific tractography could help in the determination of the best stimulating site, that is STN or GPi.

Bibliography

[1] Lorraine V Kalia and Anthony E Lang. Parkinson's disease. The Lancet, 386(9996):896–912, aug 2015.

[2] Michael J. Frank. Dynamic Dopamine Modulation in the Basal Ganglia: A Neurocomputational Account of Cognitive Deficits in Medicated and Nonmedicated Parkinsonism. Journal of Cognitive Neuroscience, 17(1):51–72, jan 2005.

[3] Izhar Bar-Gad, Genela Morris, and Hagai Bergman. Information processing, dimensionality reduction and reinforcement learning in the basal ganglia. Progress in Neurobiology, 71(6):439–473, dec 2003.

[4] O Hornykiewicz and S J Kish. Biochemical pathophysiology of Parkinson's disease. Advances in neurology, 45:19–34, 1987.

[5] European Brain Council: Parkinson's disease.

[6] Lonneke ML de Lau and Monique MB Breteler. Epidemiology of Parkinson's disease. The Lancet Neurology, 5(6):525–535, jun 2006.

[7] Stephen K Van Den Eeden, Caroline M Tanner, Allan L Bernstein, Robin D Fross, Amethyst Leimpeter, Daniel A Bloch, and Lorene M Nelson. Incidence of Parkinson's disease: variation by age, gender, and race/ethnicity. American journal of epidemiology, 157(11):1015–22, jun 2003.

[8] E. R. Dorsey, R. Constantinescu, J. P. Thompson, K. M. Biglan, R. G. Holloway, K. Kieburtz, F. J. Marshall, B. M. Ravina, G. Schifitto, A. Siderowf, and C. M. Tanner. Projected number of people with Parkinson disease in the most populous nations, 2005 through 2030. Neurology, 68(5):384–386, jan 2007.

[9] Dale Purves. Neuroscience. New York : Oxford University Press, 2018, sixth edition, 2018.

[10] Atsushi Nambu, Hironobu Tokuno, and Masahiko Takada. Functional significance of the cortico–subthalamo–pallidal 'hyperdirect' pathway. Neuroscience Research, 43(2):111–117, jun 2002.

[11] Eli J. Müller and Peter A. Robinson. Quantitative theory of deep brain stimulation of the subthalamic nucleus for the suppression of pathological rhythms in Parkinson's disease. PLoS Computational Biology, 14(5):1–20, 2018.

[12] Tjitske Heida and Julien Modolo. Models of deep brain stimulation. Scholarpedia, 12(2017):1–18, 2017.

[13] H Bergman, T Wichmann, and M R DeLong. Reversal of experimental parkinsonism by lesions of the subthalamic nucleus. Science (New York, N.Y.), 249(4975):1436–8, sep 1990.

[14] John Gardner. A history of deep brain stimulation: Technological innovation and the role of clinical assessment tools. Social Studies of Science, 43(5):707–728, oct 2013.

[15] Martijn Figee, Judy Luigjes, Ruud Smolders, Carlos-Eduardo Valencia-Alfonso, Guido van Wingen, Bart de Kwaasteniet, Mariska Mantione, Pieter Ooms, Pelle de Koning, Nienke Vulink, Nina Levar, Lukas Droge, Pepijn van den Munckhof, P Richard Schuurman, Aart Nederveen, Wim van den Brink, Ali Mazaheri, Matthijs Vink, and Damiaan Denys. Deep brain stimulation restores frontostriatal network activity in obsessive-compulsive disorder. Nature Neuroscience, 16(4):386–387, apr 2013.

[16] Paul Boon, Kristl Vonck, Veerle De Herdt, Annelies Van Dycke, Maarten Goethals, Lut Goossens, Michel Van Zandijcke, Tim De Smedt, Isabelle Dewaele, Rik Achten, Wytse Wadman, Frank Dewaele, Jacques Caemaert, and Dirk Van Roost. Deep Brain Stimulation in Patients with Refractory Temporal Lobe Epilepsy. Epilepsia, 48(8):1551–1560, mar 2007.

[17] Marie Vidailhet, Laurent Vercueil, Jean-Luc Houeto, Pierre Krystkowiak, Alim-Louis Benabid, Philippe Cornu, Christelle Lagrange, Sophie Tézenas du Montcel, Didier Dormont, Sylvie Grand, Serge Blond, Olivier Detante, Bernard Pillon, Claire Ardouin, Yves Agid, Alain Destée, and Pierre Pollak. Bilateral Deep-Brain Stimulation of the Globus Pallidus in Primary Generalized Dystonia. New England Journal of Medicine, 352(5):459–467, feb 2005.

[18] Michael S Okun. Deep-Brain Stimulation for Parkinson's Disease. New England Journal of Medicine, 367(16):1529–1538, oct 2012.

[19] Mikkel V. Petersen, Torben E. Lund, Niels Sunde, Jesper Frandsen, Frederikke Rosendal, Niels Juul, and Karen Østergaard. Probabilistic versus deterministic tractography for delineation of the cortico-subthalamic hyperdirect pathway in patients with Parkinson disease selected for deep brain stimulation. Journal of Neurosurgery, 126(5):1657–1668, 2017.

[20] Donatus Cyron. Mental Side Effects of Deep Brain Stimulation (DBS) for Movement Disorders: The Futility of Denial. Frontiers in Integrative Neuroscience, 10:17, 2016.

[21] Yoshihisa Tachibana, Hirokazu Iwamuro, Hitoshi Kita, Masahiko Takada, and Atsushi Nambu. Subthalamo-pallidal interactions underlying parkinsonian neuronal oscillations in the primate basal ganglia. European Journal of Neuroscience, 34(9):1470–1484, nov 2011.

[22] Alex Pavlides, S. John Hogan, and Rafal Bogacz. Computational Models Describing Possible Mechanisms for Generation of Excessive Beta Oscillations in Parkinson's Disease. PLoS Computational Biology, 11(12):1–29, 2015.

[23] Osamu Shouno, Yoshihisa Tachibana, Atsushi Nambu, and Kenji Doya. Computational Model of Recurrent Subthalamo-Pallidal Circuit for Generation of Parkinsonian Oscillations. Frontiers in Neuroanatomy, 11:21, mar 2017.

[24] Eli J. Müller and Peter A. Robinson. Suppression of Parkinsonian Beta Oscillations by Deep Brain Stimulation: Determination of Effective Protocols. Frontiers in Computational Neuroscience, 12(December):1–16, 2018.

[25] S Mori and J Zhang. Diffusion Tensor Imaging. Current Protocols in Magnetic Resonance Imaging, pages A6.4.1 – A6.4.12, 2009.

[26] P Douek, R Turner, J Pekar, N Patronas, and D Le Bihan. MR color mapping of myelin fiber orientation. Journal of computer assisted tomography, 15(6):923–929, 1991.

[27] P Mukherjee, J I Berman, C P Hess, and R G Henry. Diffusion Tensor MR Imaging and Fiber Tractography : Theoretic Underpinnings. American Journal of Neuroradiology, 27(5):1040–1045, 2008.

[28] Brian J. Jellison, Aaron S. Field, Joshua Medow, Mariana Lazar, M. Shariar Salamat, and Andrew L. Alexander. Diffusion Tensor Imaging of Cerebral White Matter: A Pictorial Review of Physics, Fiber Tract Anatomy, and Tumor Imaging Patterns. American Journal of Neuroradiology, 23(1):67–75, 2004.

[29] Jacques-Donald Tournier, Susumu Mori, and Alexander Leemans. Diffusion tensor imaging and beyond. Magnetic Resonance in Medicine, 65(6):1532–1556, jun 2011.

[30] Heidi Johansen-Berg and Timothy E J Behrens. Diffusion MRI: From Quantitative Measurement to In vivo Neuroanatomy. Academic Press, San Diego, second edition, 2014.

[31] Eleftherios Garyfallidis. Towards an accurate brain tractography. PhD thesis, University of Cambridge, may 2012.

[32] Documentation - DSI Studio.

[33] Brian D Coley. Caffey's pediatric diagnostic imaging, 2019.

[34] Fang-Cheng Yeh, Van Jay Wedeen, and Wen-Yih Isaac Tseng. Generalized q-Sampling Imaging. IEEE Transactions on Medical Imaging, 29(9):1626–1635, sep 2010.

[35] Fang-Cheng Yeh, Li Liu, T. Kevin Hitchens, and Yijen L. Wu. Mapping immune cell infiltration using restricted diffusion MRI. Magnetic Resonance in Medicine, 77(2):603–612, feb 2017.

[36] Fang-Cheng Yeh and Wen-Yih Isaac Tseng. NTU-90: A high angular resolution brain atlas constructed by q-space diffeomorphic reconstruction. NeuroImage, 58(1):91–99, sep 2011.

[37] N Tzourio-Mazoyer, B Landeau, D Papathanassiou, F Crivello, O Etard, N Delcroix, B Mazoyer, and M Joliot. Automated anatomical labeling of activations in SPM using a macroscopic anatomical parcellation of the MNI MRI single-subject brain. NeuroImage, 15(1):273–89, 2002.

[38] Hsiang Yuan Lin, Alistair Perry, Luca Cocchi, James A. Roberts, Wen Yih Isaac Tseng, Michael Breakspear, and Susan Shur Fen Gau. Development of frontoparietal connectivity predicts longitudinal symptom changes in young people with autism spectrum disorder. Translational Psychiatry, 9(1), 2019.

[39] Fang Cheng Yeh, Timothy D. Verstynen, Yibao Wang, Juan C. Fernández-Miranda, and Wen Yih Isaac Tseng. Deterministic diffusion fiber tracking improved by quantitative anisotropy. PLoS ONE, 8(11):1–16, 2013.

[40] Paolo Gelosa, Elisabetta Bonfanti, Laura Castiglioni, José Maria Delgado-Garcia, Agnès Gruart, Lucia Fontana, Marco Gotti, Elena Tremoli, Davide Lecca, Marta Fumagalli, Mauro Cimino, Ludwig Aigner, Maria P. Abbracchio, and Luigi Sironi. Improvement of fiber connectivity and functional recovery after stroke by montelukast, an available and safe anti-asthmatic drug. Pharmacological Research, 142(July 2018):223–236, 2019.

[41] Fang-Cheng Yeh, Sandip Panesar, Jessica Barrios, David Fernandes, Kumar Abhinav, Antonio Meola, and Juan C. Fernandez-Miranda. Improved Accuracy of Diffusion MRI Tractography Using Topology-Informed Pruning (TIP). bioRxiv, page 338624, jun 2018.

[42] Andreas Horn and Andrea A. Kühn. Lead-DBS: A toolbox for deep brain stimulation electrode localizations and visualizations. NeuroImage, 107:127–135, feb 2015.

[43] Andreas Horn, Ningfei Li, Till A. Dembek, Ari Kappel, Chadwick Boulay, Siobhan Ewert, Anna Tietze, Andreas Husch, Thushara Perera, Wolf-Julian Neumann, Marco Reisert, Hang Si, Robert Oostenveld, Christopher Rorden, Fang-Cheng Yeh, Qianqian Fang, Todd M. Herrington, Johannes Vorwerk, and Andrea A. Kühn. Lead-DBS v2: Towards a comprehensive pipeline for deep brain stimulation imaging. NeuroImage, 184:293–316, jan 2019.

[44] Brian B. Avants, Nick Tustison, and Gang Song. Advanced Normalization Tools (ANTS) V1.0. Insight journal, page 35, 2009.

[45] SPM12 - Statistical Parametric Mapping.

[46] Lead-DBS Manual.

[47] Andreas Husch, Mikkel V Petersen, Peter Gemmar, Jorge Goncalves, and Frank Hertel. PaCER - A fully automated method for electrode trajectory and contact reconstruction in deep brain stimulation. NeuroImage. Clinical, 17:80–89, 2018.

[48] Johannes Vorwerk, Robert Oostenveld, Maria Carla Piastra, Lilla Magyari, and Carsten H. Wolters. The FieldTrip-SimBio pipeline for EEG forward solutions. BioMedical Engineering OnLine, 17(1):37, dec 2018.

[49] Alexander Sitz, Mauritius Hoevels, Alexandra Hellerbach, Andreas Gierich, Klaus Luyken, Till A. Dembek, Martin Klehr, Jochen Wirths, Veerle Visser-Vandewalle, and Harald Treuer. Determining the orientation angle of directional leads for deep brain stimulation using computed tomography and digital x-ray imaging: A phantom study. Medical Physics, 44(9):4463–4473, sep 2017.

[50] Gerd Tinkhauser, Alek Pogosyan, Ines Debove, Andreas Nowacki, Syed Ahmar Shah, Kathleen Seidel, Huiling Tan, John-Stuart Brittain, Katrin Petermann, Lazzaro di Biase, Markus Oertel, Claudio Pollo, Peter Brown, and Michael Schuepbach. Directional local field potentials: A tool to optimize deep brain stimulation. Movement Disorders, 33(1):159–164, jan 2018.

[51] Paula Sanz-Leon, Peter A. Robinson, Stuart A. Knock, Peter M. Drysdale, Romesh G. Abeysuriya, Felix K. Fung, Chris J. Rennie, and Xuelong Zhao. NFTsim: Theory and Simulation of Multiscale Neural Field Dynamics. PLOS Computational Biology, 14(8):e1006387, aug 2018.

[52] Brain Dynamics Group University of Sydney. NFTsim User Guide, 2015.

[53] Wolf Julian Neumann, Henning Schroll, Ana Luisa De Almeida Marcelino, Andreas Horn, Siobhan Ewert, Friederike Irmen, Patricia Krause, Gerd Helge Schneider, Fred Hamker, and Andrea A. Kühn. Functional segregation of basal ganglia pathways in Parkinson's disease. Brain, 141(9):2655–2669, 2018.

[54] Kabilar Gunalan, Ashutosh Chaturvedi, Bryan Howell, Yuval Duchin, Scott F. Lempka, Remi Patriat, Guillermo Sapiro, Noam Harel, and Cameron C. McIntyre. Creating and parameterizing patient-specific deep brain stimulation pathway-activation models using the hyperdirect pathway as an example. PLoS ONE, 12(4):1–19, 2017.

[55] Klaus H. Maier-Hein, Peter F. Neher, Jean-Christophe Houde, Marc-Alexandre Côté, Eleftherios Garyfallidis, Jidan Zhong, Maxime Chamberland, Fang-Cheng Yeh, Ying-Chia Lin, Qing Ji, Wilburn E. Reddick, John O. Glass, David Qixiang Chen, Yuanjing Feng, Chengfeng Gao, Ye Wu, Jieyan Ma, H. Renjie, Qiang Li, Carl-Fredrik Westin, Samuel Deslauriers-Gauthier, J. Omar Ocegueda González, Michael Paquette, Samuel St-Jean, Gabriel Girard, François Rheault, Jasmeen Sidhu, Chantal M. W. Tax, Fenghua Guo, Hamed Y. Mesri, Szabolcs Dávid, Martijn Froeling, Anneriet M. Heemskerk, Alexander Leemans, Arnaud Boré, Basile Pinsard, Christophe Bedetti, Matthieu Desrosiers, Simona Brambati, Julien Doyon, Alessia Sarica, Roberta Vasta, Antonio Cerasa, Aldo Quattrone, Jason Yeatman, Ali R. Khan, Wes Hodges, Simon Alexander, David Romascano, Muhamed Barakovic, Anna Auría, Oscar Esteban, Alia Lemkaddem, Jean-Philippe Thiran, H. Ertan Cetingul, Benjamin L. Odry, Boris Mailhe, Mariappan S. Nadar, Fabrizio Pizzagalli, Gautam Prasad, Julio E. Villalon-Reina, Justin Galvis, Paul M. Thompson, Francisco De Santiago Requejo, Pedro Luque Laguna, Luis Miguel Lacerda, Rachel Barrett, Flavio Dell'Acqua, Marco Catani, Laurent Petit, Emmanuel Caruyer, Alessandro Daducci, Tim B. Dyrby, Tim Holland-Letz, Claus C. Hilgetag, Bram Stieltjes, and Maxime Descoteaux. The challenge of mapping the human connectome based on diffusion tractography. Nature Communications, 8(1):1349, dec 2017.

[56] Heidi Johansen-Berg. Structural Plasticity: Rewiring the Brain. Current Biology, 17(4):R141–R144, feb 2007.

[57] S. Li, G. W. Arbuthnott, M. J. Jutras, J. A. Goldberg, and D. Jaeger. Resonant Antidromic Cortical Circuit Activation as a Consequence of High-Frequency Subthalamic Deep-Brain Stimulation. Journal of Neurophysiology, 98(6):3525–3537, dec 2007.

[58] Qian Li, Ya Ke, Danny C W Chan, Zhong-Ming Qian, Ken K L Yung, Ho Ko, Gordon W Arbuthnott, and Wing-Ho Yung. Therapeutic deep brain stimulation in Parkinsonian rats directly influences motor cortex. Neuron, 76(5):1030–41, dec 2012.

[59] Viviana Gradinaru, Murtaza Mogri, Kimberly R. Thompson, Jaimie M. Henderson, and Karl Deisseroth. Optical Deconstruction of Parkinsonian Neural Circuitry. Science, 324(5925):354–359, apr 2009.

[60] Teresa H. Sanders and Dieter Jaeger. Optogenetic stimulation of cortico-subthalamic projections is sufficient to ameliorate bradykinesia in 6-ohda lesioned mice. Neurobiology of Disease, 95:225–237, nov 2016.

[61] Elena Moro, Andres M. Lozano, Pierre Pollak, Yves Agid, Stig Rehncrona, Jens Volkmann, Jaime Kulisevsky, Jose A. Obeso, Alberto Albanese, Marwan I. Hariz, Niall P. Quinn, Jans D. Speelman, Alim L. Benabid, Valerie Fraix, Alexandre Mendes, Marie-Laure Welter, Jean-Luc Houeto, Philippe Cornu, Didier Dormont, Annalena L. Tornqvist, Ron Ekberg, Alfons Schnitzler, Lars Timmermann, Lars Wojtecki, Andres Gironell, Maria C. Rodriguez-Oroz, Jorge Guridi, Anna R. Bentivoglio, Maria F. Contarino, Luigi Romito, Massimo Scerrati, Marc Janssens, and Anthony E. Lang. Long-term results of a multicenter study on subthalamic and pallidal stimulation in Parkinson's disease. Movement Disorders, 25(5):578–586, apr 2010.

[62] Jan Herzog, Urban Fietzek, Wolfgang Hamel, Andre Morsnowski, Frank Steigerwald, Bettina Schrader, Dieter Weinert, Gerd Pfister, Dieter Müller, Hubertus M. Mehdorn, Günther Deuschl, and Jens Volkmann. Most effective stimulation site in subthalamic deep brain stimulation for Parkinson's disease. Movement Disorders, 19(9):1050–1054, sep 2004.

[63] Scott F Lempka and Cameron C McIntyre. Theoretical analysis of the local field potential in deep brain stimulation applications. PloS one, 8(3):e59839, 2013.

[64] Ben Jeurissen, Alexander Leemans, Jacques-Donald Tournier, Derek K Jones, and Jan Sijbers. Investigating the prevalence of complex fiber configurations in white matter tissue with diffusion MRI. Human brain mapping, 34(11):2747–2766, nov 2013.

[65] Bethany R. Isaacs, Birte U. Forstmann, Yasin Temel, and Max C. Keuken. The Connectivity Fingerprint of the Human Frontal Cortex, Subthalamic Nucleus, and Striatum. Frontiers in Neuroanatomy, 12(July):1–18, 2018.